UNCLASSIFIED

NAA-SR-9754
COPY
80 PAGES

SNAP 10A REACTOR NUCLEAR ANALYSIS

(Title Unclassified)

AEC Research and Development Report

ATOMICS INTERNATIONAL
A DIVISION OF NORTH AMERICAN AVIATION, INC.

DISCLAIMER

LEGAL NOTICE

Printed in USA Price $1.45 Available from the

U. S. Atomic Energy Commission
Technical Information Extension,
P. O. Box 1001
Oak Ridge, Tennessee.

Please direct to the same address inquiries covering the procurement of other classified AEC reports.

NAA-SR-9754
SNAP REACTOR,
SNAP PROGRAM
M-3679 (38th Ed.)

SNAP 10A REACTOR NUCLEAR ANALYSIS

(Title Unclassified)

By
A.R. DAYES
W.A. FLYNN
J.P. HAWLEY

ATOMICS INTERNATIONAL
A DIVISION OF NORTH AMERICAN AVIATION, INC.
P.O. BOX 309 CANOGA PARK, CALIFORNIA

CONTRACT: AT(11-1)-GEN-8
ISSUED: JANUARY 15, 1965

DISTRIBUTION

SYSTEMS FOR NUCLEAR AUXILIARY POWER (SNAP)-REACTOR SNAP PROGRAM M-3679 (38th Ed.)

	No. of Copies
Aerojet-General Corporation (NASA)	6
Aerojet-General Corporation, Sacramento	1
Aerojet-General Nucleonics	1
Aerojet-General Nucleonics (NASA)	1
Aeronautical Systems Division	2
Aerospace Corporation	1
Aerospace Test Wing (AFSC)	1
Air Force Surgeon General	1
Air Force Weapons Laboratory	2
Air University Library	1
AiResearch Manufacturing Company, Phoenix	1
Allison Division – GMC	1
Argonne National Laboratory	1
Army Ballistic Research Laboratories	1
Army Missile Command	1
Army Weapons Command	1
ARO, Inc.	1
Avco Corporation	1
Battelle Memorial Institute	1
Bendix Corporation (AF)	1
Brookhaven National Laboratory	1
Bureau of Naval Weapons	2
Bureau of Ships	2
Bureau of Yards and Docks	1
California Patent Group	1
Central Intelligence Agency	1
Chicago Patent Group	1
Defense Atomic Support Agency, Sandia	1
Department of the Army	1
Director of Defense Research and Engineering (OAP)	1
Douglas Aircraft Company, Inc., Newport Beach	1
Edgerton, Germeshausen and Grier, Inc., Goleta	1
Electro-Optical Systems, Inc.	1
Foreign Technology Division (AFSC)	1
General Atomic Division	1
General Dynamics/Astronautics (AF)	1
General Dynamics/Fort Worth	1
General Electric Company, Cincinnati	1
General Electric Company (FPD)	2
General Electric Company (MSVD)	1
General Electric Company, Richland	2
General Electric Company, San Jose	1
Jet Propulsion Laboratory	2
Johns Hopkins University (APL)	1
Lockheed-Georgia Company	1
Lockheed Missiles and Space Company	1
Los Alamos Scientific Laboratory	1
Martin-Marietta Corporation, Denver	1
Monsanto Dayton Laboratory	1
Mound Laboratory	1
NASA Ames Research Center	1
NASA Goddard Space Flight Center	2
NASA Langley Research Center	1
NASA Lewis Research Center	7
NASA Manned Spacecraft Center	1
NASA Marshall Space Flight Center	1
NASA Scientific and Technical Information Facility	3
National Aeronautics and Space Administration, Washington	2
NASA Western Operations Office	1
Naval Air Development Center	1
Naval Ordnance Laboratory	2
Naval Postgraduate School	1
Naval Radiological Defense Laboratory	1
Naval Research Laboratory	2
Naval Underwater Ordnance Station	1
Navy Marine Engineering Laboratory	1
New York Operations Office	1
New York Operations Office, Canel Project Office	1
Nuclear Metals, Inc.	1
Office of Naval Research	2
Office of the Assistant General Counsel for Patents (AEC)	1
Office of the Chief of Engineers	1
Office of the Chief of Naval Operations	3
Office of the Chief of Naval Operations (OP-03EG)	2
Office of the Chief of Transportation	1
Phillips Petroleum Company (NRTS)	4
Pratt and Whitney Aircraft Division	1
Pratt and Whitney Aircraft Division (NASA)	1
Rand Corporation	1
Sandia Corporation	1
School of Aerospace Medicine	1
Union Carbide Corporation (ORNL)	8
United Nuclear Corporation (NDA)	1
USAF Headquarters	1
University of California, Livermore	1
Westinghouse Electric Corporation, Lima	1
Westinghouse Electric Corporation, Lima (AF)	1
Westinghouse Electric Corporation (NASA)	1
White Sands Missile Range	2
Division of Technical Information Extension	40
AI Library (Includes 2 copies to CPAO, 2 copies to AEC, Washington, 2 copies to COO)	57

CONTENTS

TABLES

FIGURES

FIGURES

BLANK

ABSTRACT

A physical description of the SNAP 10A reactor and a description of the calculational models employed for nuclear analysis are presented. Analytical methods and sources of nuclear constants are discussed. Where available, experimental results are compared to analytical results.

The nuclear characteristics of the reactor are tabulated and discussed. Reactor safety devices are described and their analysis is presented. Analysis of the first ground test reactor, S10FS-1, is also included.

BLANK

I. INTRODUCTION

The SNAP 10A reactor (System for Nuclear Auxiliary Power) is to be the heat source for a thermoelectric power conversion system. This system will supply power for earth satellites and other space vehicles. The operation of a reactor in a space environment imposes the requirements of remote control, high reliability, compactness, and long operating life.

High reliability for static reactor control for an extended period of time demands a detailed knowledge of the physics of the reactor. To determine the inherent qualities of the SNAP 10A design, an extensive program of computation and experimentation has been performed. This report is a compendium of the results and conclusions of this program. Information that has been gathered and deemed necessary for the successful operation of the reactor in space is included.

The calculations described herein were generally performed using the IBM 709, 7090, and 7094 digital computers. Experimental data was gathered from the SNAP Experimental Reactor (SER), the SNAP 2 Development Reactor (S2DR), the first Ground Test Reactor (S10FS-1), and the SNAP Critical Assemblies SCA-4A, -4B, and -4C.

BLANK

II. DESCRIPTION OF SNAP 10A SYSTEM

A. PHYSICAL DESCRIPTION OF SNAP 10A SYSTEM

1. General Description

The SNAP 10A reactor was designed to be employed as a heat source for a thermoelectric power conversion system. The assembled SNAP 10A system is shown in Figure 1. The thermoelectric power conversion system is designed to supply a minimum of 500 watts of electrical power for 1 year of continuous unattended operation.

After successful attainment of orbit has been verified, the reactor will be brought to its steady-state operating conditions by insertion of the beryllium control drums which make up part of the reactor-reflector. Following initiation of reactor startup there will be 72 hours of active control during which time the beryllium control drums will be inserted whenever the reactor coolant outlet temperature drops below a set point. Active control is then terminated and the reactor outlet temperature is maintained approximately constant over the remainder of the 1-year operating period through nuclear mechanisms which are inherent in the reactor.

The conversion of thermal to electric energy is accomplished by the maintenance of a temperature difference across germanium-silicon alloy thermoelectric converters. These converters are located between the NaK coolant pipes and the truncated conical radiator surface. Eutectic sodium-potassium alloy (NaK-78) is employed as the reactor coolant. The coolant is pumped through the system by a thermoelectric pump which is located in the coolant outlet line directly above the reactor. The pump utilizes its own thermoelectric converter to generate sufficient electrical energy to pump the coolant through the closed loop system.

2. Reactor Description

A cutaway view of the SNAP 10A reactor is shown in Figure 2, and pertinent design and nuclear characteristics are summarized in Table 1. As indicated in the tabulation, the SNAP 10A reactor is fueled with 93% enriched uranium. The uranium is dispersed in a zirconium-hydride moderator which contains 10 wt % U. The 37 fuel-moderator rods, each 12-1/4 in. long, are

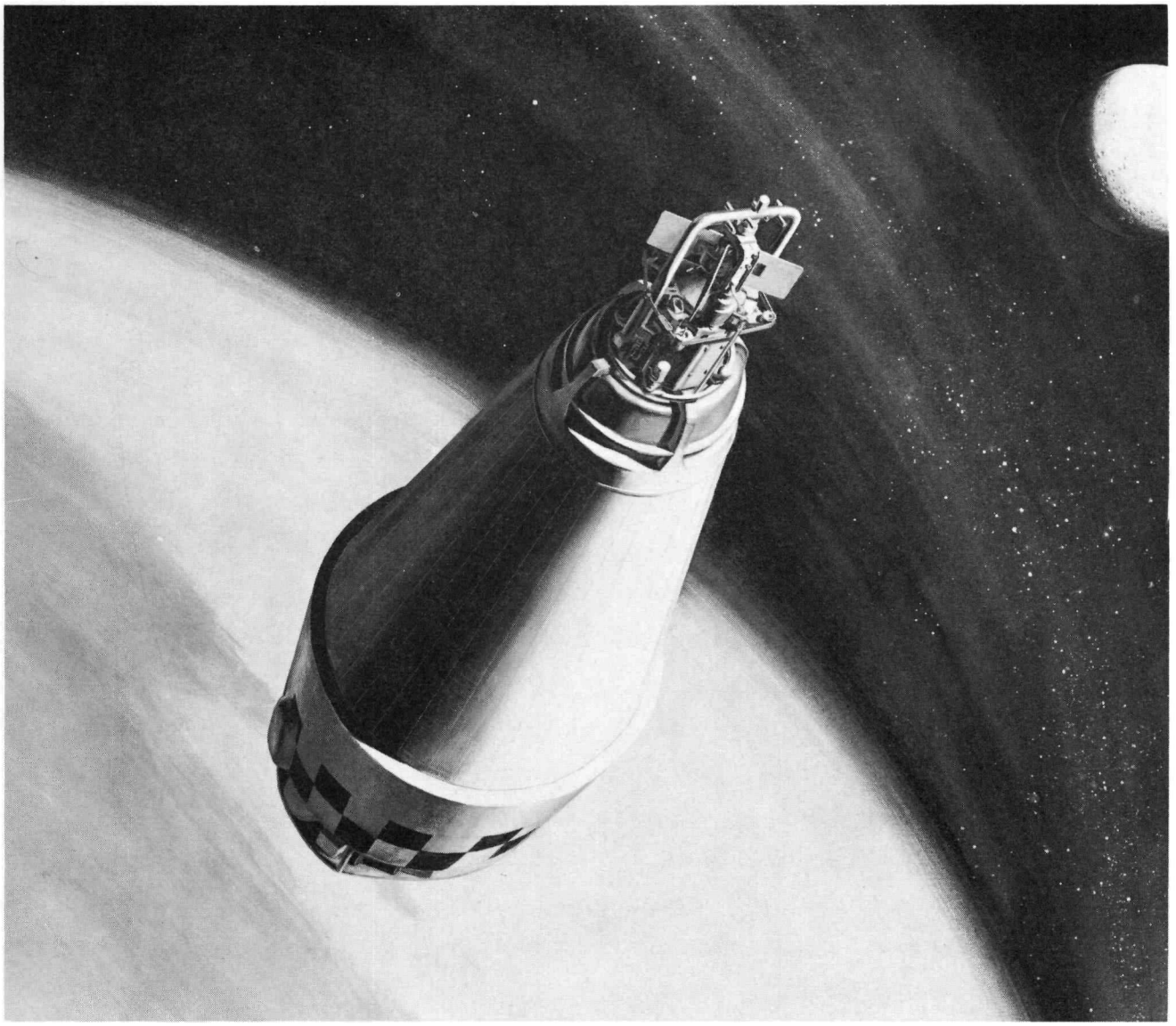

2-15-63 7561-0282

Figure 1. SNAP 10A Reactor-Reflector and Converter Assembly

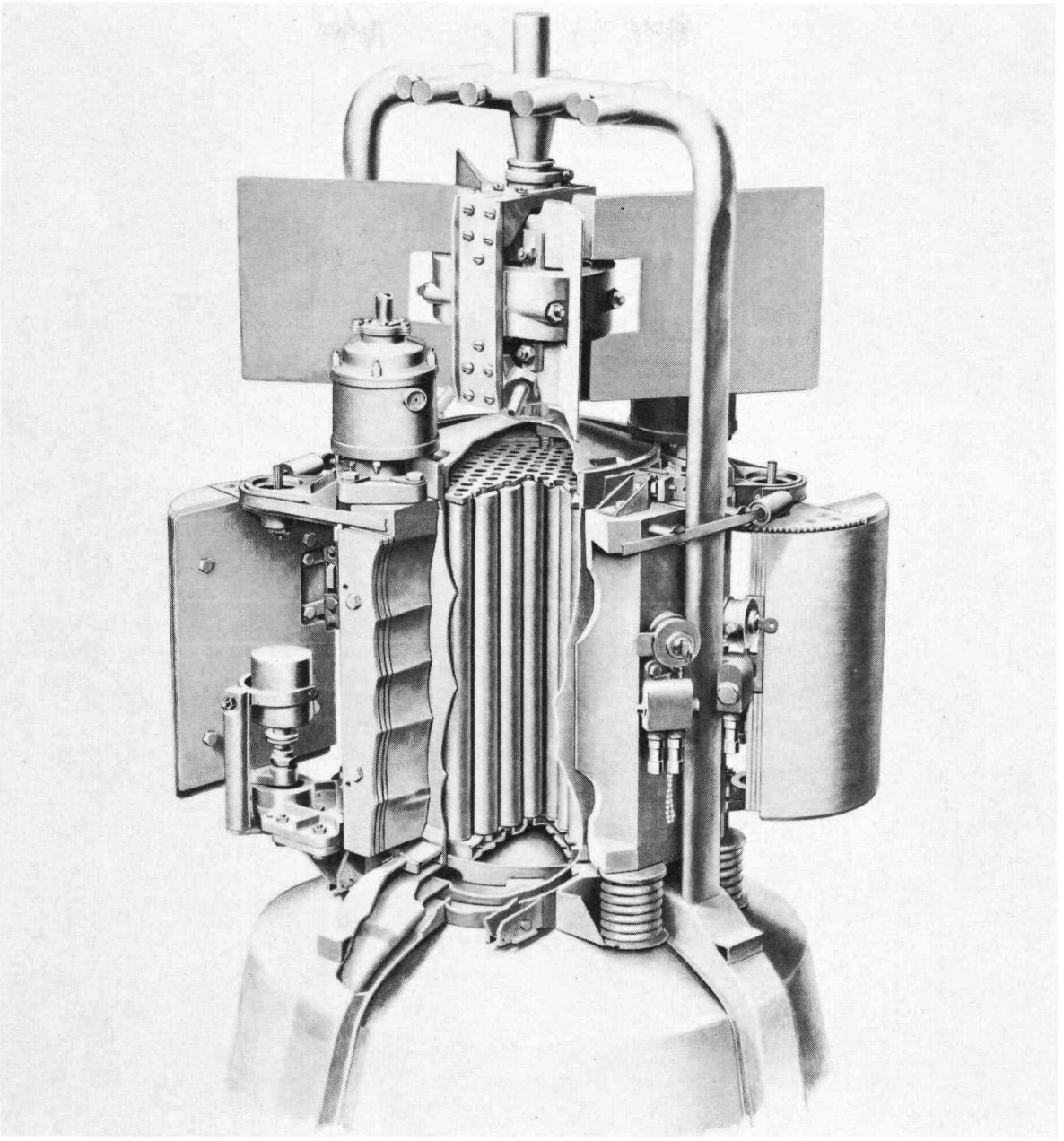

5-17-62 7580-10512C

Figure 2. Cutaway View of Reactor-Reflector and Pump Assembly

TABLE 1

SNAP 10A REACTOR CHARACTERISTICS

COMPONENTS	Component Dimensions and Materials	
Radial		
Core (hexagonal fuel rod array)	Diameter (in.) across corners	8.81
	Diameter (in.) across flats	7.80
Fuel elements	Number of elements	37
	Pitch of elements (in.)	1.26
	Diameter of U-Zr H Fuel (in.)	1.21
	Outside diameter of element (in.)	1.25
	Cladding thickness (in.) (Hastelloy-N)	0.015
	Ceramic thickness (in)	0 003
Fuel alloy	Uranium enrichment (% U^{235})	93
	U^{235} per element (gm)	128.4
	H_2 concentration in fuel (atoms H_2/cc fuel moderator)	6.35 ± 0.03
	U wt % before hydriding	10.15
	U wt % after hydriding	9.97
	Zr wt % after hydriding	88.23
	H wt % after hydriding	1.8
Internal reflectors	6 pieces metallic Be fitted between fuel array and vessel	
Vessel	Stainless steel 316	
	Inside diameter (in.)	8.875
	Outside diameter (in.)	8.939
Gap between reflector and vessel	FS-1 (in.)	0.045
	FS-3, 4, and 5 (in.)	0.055
Main Be reflector	Average thickness (in.)	
	FS-1	1.991
	FS-3, 4, and 5	1.981
	Height (in.)	12.25
Axial		
Tophead	Stainless steel 316	
Plenum-upper	NaK ($in.^3$)	50.8
Gridplate-upper	Stainless steel 316	
	thickness (in.)	0.125
	diameter (in.)	8.830

COMPONENTS	Component Dimensions and Materials	
Core	Active length of fuel rods (in.)	12.25
	Length of elements (in)	12.45
	End plugs - Hastelloy-N	
Gridplate-lower	Stainless steel 316 sandwich construction	
	thickness (in.)	0.50
	diameter (in.)	8.75
Plenum-lower	NaK in gridplate ($in.^3$)	20.8
	NaK in plenum ($in.^3$)	74.2
Vessel bottom	Stainless steel 316	
Parameters	Parameter Values	
Prompt neutron lifetime (μ sec)	6.5	
Median fission energy (ev)	0.12	
Effective delayed neutron fraction (β_{eff})	0.008	
Average isothermal temperature coefficient (¢/°F)	-0.245	
Power coefficient (¢/kw)	-0.17	
Power level, average (kw)	39.5	
Power Distribution and Fluxes	Power Distribution, Flux Values	
Overall peak-to-average power ratio	1.9	
Radial peak-to-average power ratio	1.3	
Axial peak-to-average power ratio	1.45	
Thermal flux (neutron energy less than 0.4 ev)		
Core average (neutrons/cm^2/sec)	2.5×10^{11}	
Peak (neutrons/cm^2/sec)	4.7×10^{11}	
Fast neutron leakage (>0.1 Mev) (neutrons/sec)	1×10^{15}	

clad in 15-mil-thick Hastelloy-N. The inside wall of each cladding tube is coated with a ceramic material which impedes the loss of hydrogen from the element.

To encapsulate fuel rods in the cladding tubes, plugs are welded in each end of the tubes. Each end plug contains an indexing pin approximately 1/4 in. in diameter. The 37 fuel elements are arranged in a hexagonal pattern and the interstices between the fuel elements form channels for coolant flow.

The fuel elements are held in place at top and bottom by stainless steel gridplates. These perforated plates support and stabilize the fuel elements while permitting coolant flow. The lower gridplate is orificed to control the radial distribution of flow through the core. The top gridplate is 1/8 in. thick while the bottom plate, which is of sandwich construction, has an overall thickness of 1/2 in. The top gridplate is restrained from movement in the axial direction by 12 springs which are compressed against the top head of the reactor. The bottom gridplate is supported by a flange which is spotwelded to the inside surface of the vessel.

Since the fuel element array is hexagonal and the reactor vessel is circular, there are relatively large open regions between the "flat" surfaces of the hexagon and the vessel. Six beryllium pieces are fitted into these regions, providing additional neutron reflection and preventing by-pass flow. The beryllium internal reflector pieces are curved to fit the reactor vessel and mesh with the surface of the fuel rod array. These internal beryllium reflectors are held in position by indexing pins inserted into the gridplates. The coolant outlet and inlet plenums are located between the top gridplate and the top head and between the bottom gridplate and the bottom of the vessel, respectively.

The radial surface of the reactor vessel is surrounded by the main beryllium reflector, as shown in Figure 3. The reflector is approximately octagonal in cross section when the control drums are inserted and its length is the same as the length of the active fuel rod (i.e., 12-1/4 in.). Four control drums, approximately 10 in. long and semicircular in cross section, make up four sides of the reflector. The drums can be rotated into the reflector, increasing core reactivity through reduction of the neutron leakage. All four control drums and two of the fixed reflector surfaces (those located 90° from the reflector separation plane) can be shimmed using 1/8-in.-thick beryllium plates. A maximum

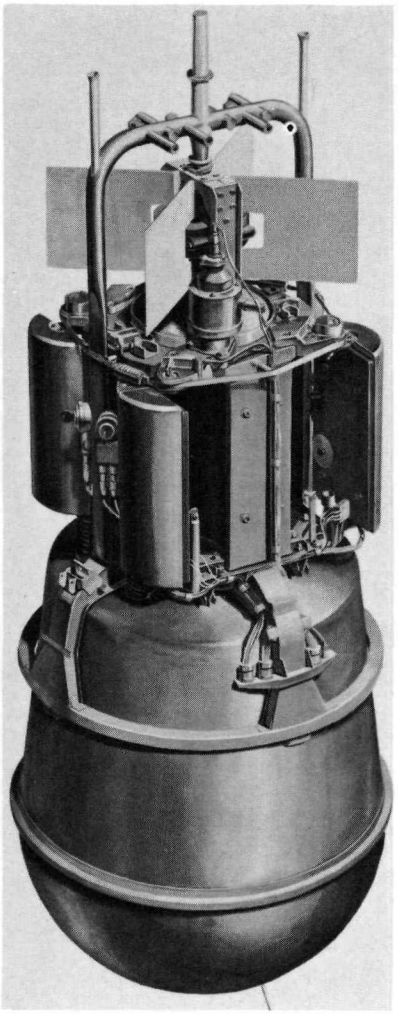

8-1-63 7523-0017

Figure 3. SNAP 10A Reactor and Shield

of 3 shims, or 3/8 in. of beryllium, can be added to the reflector or drums. Both control drum worth and reflector worth can be increased by this method.

B. NUCLEAR MODEL

The computer codes and calculational methods employed in analyses of reactors require representation of the reactor by an idealized model. Two SNAP 10A models were formulated, one for calculation of radial effects and the other for axial calculations. Each model consists of a number of homogenized regions. Since fuel and moderator are intimately mixed in these cores, the assumption of homogenization introduces very little error into analyses of uranium-zirconium-hydride fueled reactors.

Compact reactors are characterized by relatively high neutron leakage from the core and other regions. Leakage in the transverse direction is simulated in the idealized one-dimensional models by employing an appropriate buckling term or by adjusting the absorption in each region to account for the neutrons that are lost.

1. Radial Model

The radial model is divided into three regions. Region 1 of Figure 4 for the radial case describes the active core. The height of the region is taken as the active length of the fuel rods. The radius of the idealized core region was determined by first calculating the area of the hexagon formed by connecting the centers of the six rods surrounding the center rod (Figure 5). This area is equal to the cross sectional area of three rods plus the associated coolant flow area. Since there are 37 elements in the core, this area represents 3/37 of the cross sectional area of Region 1. Components homogenized in this region include the fuel rods, the cladding tubes, and the NaK coolant.

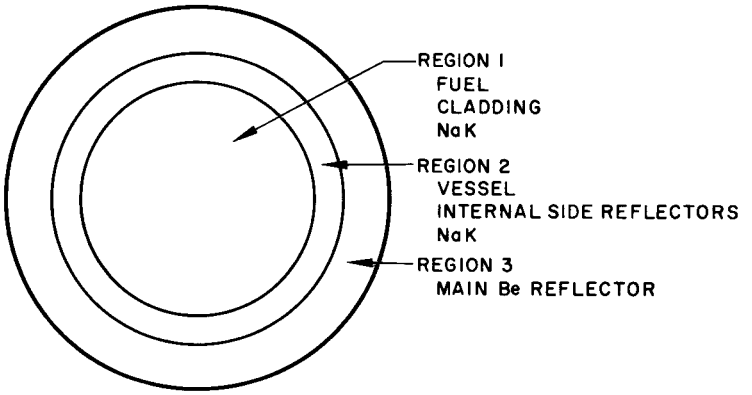

Figure 4. Radial Analytical Reactor Model

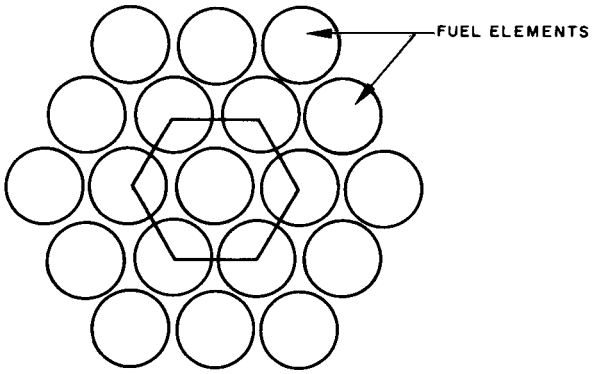

Figure 5. Cross Section of Unit Cell Used for Calculation of Active Core Radius

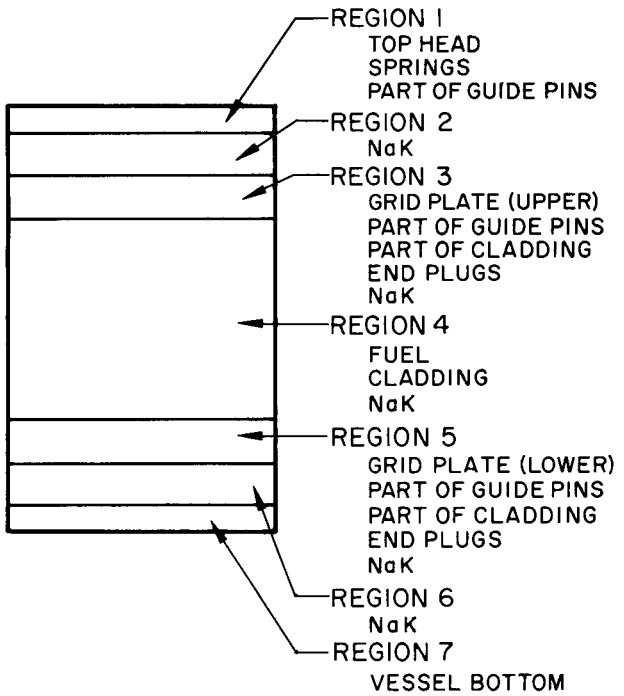

Figure 6. Axial Analytical Reactor Model

The internal reflectors and the reactor vessel were placed within Region 2 of Figure 4. The outer radius of this region is identical to the inside radius of the main reflector assembly. The gap between the vessel and the external reflector was homogenized with the materials in Region 2. As discussed in III. C. 1. c, this gap width differs for various specific SNAP 10A reactors.

The cross sectional area of the reflector assembly with all drums inserted was used to calculate the outer radius of the idealized cylindrical annulus making up Region 3 of Figure 4.

2. Axial Model

The axial model has seven regions. The radius was taken to be equal to the radius of the core region (Region 1) of the radial case. Region 1 of Figure 6 is a cylindrical slab of thickness sufficient to contain all the material of the top head, gridplate holddown springs, and that part of the fuel element end pins which lie within the core radius and above the gridplates. All the NaK above the gridplate was handled in the same way to form Region 2. Regions 6 and 7, which are the lower NaK plenums and the bottom of the reactor vessel, respectively, were treated in the same manner.

Regions 3 and 5 contain not only the gridplates but also the fuel element end plugs and part of the cladding tube. Region 3 also contains part of the guides for the top gridplate holddown springs. Region 4 of the axial case is the core, and has the same composition as Region 1 of the radial case.

A summary by regions of the radial and axial model atom densities and volume fractions is presented in Tables 2 and 3, respectively.(1)

C. REACTOR CONTROL

Two separate reactor control methods — active control and static control — are employed in the SNAP 10A reactor. Active control is employed over the first 72 hours of life and is obtained by variation of the amount of neutron leakage from the reactor through control drum movements. Static control is utilized over the remainder of reactor life. Static control implies maintenance of approximately constant reactor temperature using inherent nuclear reactivity effects; no moving control devices are required.

TABLE 2

SIMPLIFIED RADIAL ANALYTICAL MODEL
(Volume Fractions and Atomic Densities SNAP 10A-FS-3, -4, and -5 Model)

Region 1			Region 2			Region 3		
Component	Volume Fraction	Atomic Density (10^{24} atoms/cc)	Component	Volume Fraction	Atomic Density (10^{24} atoms/cc)	Component	Volume Fraction	Atomic Density (10^{24} atoms/cc)
Fuel	0.830		Internal Be Reflector	0.756		Main Reflector	1.0	
U^{235}		0.001192	Be		0.090792	Be		0.120150
U^{238}		0.000090	O		0.000663	O		0.000877
H*		0.0526903*						
Zr		0.0292434	Vessel	0.065				
			Ni		0.000673			
Cladding	0.042		C		0.000026			
Ni		0.002649	Fe		0.003654			
C		0.000011	Mo		0.000082			
Fe		0.000201	Mn		0.000114			
Cr		0.000302	Cr		0.001024			
Mn		0.000034	Si		0.000084			
Mo		0.000384						
			NaK	0.041				
NaK	0.107		Na		0.000204			
Na		0.0005312	K		0.000418			
K		0.0011078						
Sm_2O_3	0.00005		Void	0.138				
Sm		0.00000132						
O		0.00000198						
Void + Ceramic Coating	0.020							

*Based on 6.35×10^{22} $\frac{\text{Atoms of Hydrogen}}{\text{cc of Fuel}}$

TABLE 3

SIMPLIFIED AXIAL ANALYTICAL MODEL
(Volume Fractions and Atomic Densities)

Region 1			Region 2			Region 3		
Component	Volume Fraction	Atomic* Density	Component	Volume Fraction	Atomic* Density	Component	Volume Fraction	Atomic* Density
Tophead	0.882		NaK	1.0		Grid-plate	0.423	
Ni		0.009101	Na		0.00494	Ni		0.004380
C		0.000353	K		0.01031	C		0.000169
Fe		0.049383				Fe		0.023779
Mo		0.001104				Mo		0.000534
Mn		0.003086				Mn		0.000742
Cr		0.013857				Cr		0.006664
Si		0.001132				Si		0.000547
Guide Pins	0.033					Guide Pins	0.001	
Ni		0.001625				Ni		0.000026
C		0.000012				C		0.0000001
Fe		0.000174				Fe		0.000003
Mo		0.000294				Mo		0.000005
Mn		0.000032				Mn		0.0000005
Cr		0.000526				Cr		0.000008
Si		0.000063				Si		0.000001
Co		0.100075				Co		0.000001
W		0.000038				W		0.000001
Springs	0.085					Cladding	0.015	
Ni		0.003569				Ni		0.000942
C		0.000031				C		0.000004
Al		0.000233				Fe		0.000071
Fe		0.000376				Mo		0.000137
Mo		0.000427				Mn		0.000012
Mn		0.000038				Cr		0.000107
Cr		0.001534				End Plugs	0.349	
Si		0.000097				Ni		0.021673
B		0.000003				C		0.000091
Co		0.000784				Fe		0.001638
Ti		0.000276				Mo		0.003147
						Mn		0.000266
						Cr		0.002463
						NaK	0.137	
						Na		0.000664
						K		0.001385
						Void	0.075	

*10^{24} atoms/cc

TABLE 3 (Continued)

SIMPLIFIED AXIAL ANALYTICAL MODEL

Region 4	Region 5			Region 6			Region 7		
	Component	Volume Fraction	Atomic* Density	Component	Volume Fraction	Atomic* Density	Component	Volume Fraction	Atomic* Density
Same as Region 1 Radial Model	Gridplate	0.224		NaK	1.0		Vessel Btm	1.0	
	Ni		0.002319	Na		0.00494	Ni		0.01011
	C		0.000090	K		0.01031	C		0.000395
	Fe		0.012592				Fe		0.05538
	Mo		0.000283				Mo		0.00124
	Mn		0.000393				Cr		0.0155
	Cr		0.003529				Mn		0.00173
	Si		0.000289				Si		0.001283
	Cladding	0.006							
	Ni		0.000368						
	C		0.0000001						
	Fe		0.000028						
	Mo		0.000053						
	Mn		0.000004						
	Cr		0.000042						
	End Plugs	0.134							
	Ni		0.008456						
	C		0.000029						
	Fe		0.000636						
	Mo		0.001221						
	Mn		0.000100						
	Cr		0.000957						
	NaK	0.607							
	Na		0.003000						
	K		0.006255						
	Void	0.029							

*10^{24} atoms/cc

Control action is initiated after a satisfactory orbit has been achieved. The two coarse control drums are immediately snapped to their in position. An electronic controller-actuator then starts to drive the two fine control drums inward at a rate of 1/2° of drum insertion every 150 sec. Drum insertion continues as the reactor achieves criticality and goes through an initial power transient. Insertion finally ceases when the coolant outlet temperature reaches its normal operating value of 1010 ± 10°F. It is expected that this temperature will be reached approximately 9 hr after receipt of the startup command.

Coolant outlet temperature is measured by resistance thermometers and thermocouples located in the NaK outlet line. The sensor is connected to an electrical relay located in the instrument compartment. During the active control period, the relay opens to activate the controller when the outlet temperature falls below the specified level. The actuator motor then moves the fine control drums inward until the desired temperature is again reached. The 150-sec time delay between successive 1/2° drum insertion steps allows the reactor temperature to respond to the increase in reactivity. During this 72-hr period, short term reactivity changes resulting from temperature and power defects, attainment of xenon equilibrium, and partial hydrogen redistribution take place.

At the end of the active control period, control drum insertion ceases and reactor temperature is maintained by means of inherent nuclear devices. Over the remainder of the year, the decrease in reactivity due to fuel depletion, fission product accumulation, completion of hydrogen redistribution and hydrogen loss from fuel elements is compensated by the increase in reactivity due to the burnup of samarium oxide prepoison. Since reactivity remains approximately constant, temperature also remains essentially constant. The relatively large negative temperature and power coefficients of the reactor also tend to stabilize temperature during the static control period.

III. COMPARISON OF SNAP 10A NUCLEAR CALCULATIONS AND EXPERIMENTS

A. CALCULATIONAL METHODS

SNAP 10A reactor calculations were usually carried out using digital computer codes. Codes based on multigroup neutron diffusion theory have been found to provide reactivity data which is in good agreement with experiments for nuclear effects occuring within the reactor core. Diffusion theory codes were therefore used extensively for examination of in-core nuclear characteristics. Computer codes based on transport theory were often used for calculation of criticality and for prediction of effects in small regions, near boundaries, and outside the reactor core. In these cases the greater accuracy of the transport theory calculations justified the expenditure of additional computer time. Hand-calculational techniques were also employed, especially during the early phases of SNAP 10A analyses, for estimation of certain reactivity-lifetime effects. The codes and methods used in nuclear analysis of SNAP 10A reactors have been described in detail in other documents. A brief description of these codes is presented below and more details will be found in the referenced reports.

AIM-6[2] — A neutron diffusion theory code with options for use of either 16 or 18 neutron energy groups and as many as 20 separate regions. It is a one-dimensional code but an option is provided for iterating in two directions for the same problem. Slab, spherical, and cylindrical geometries can be examined. AIM-6 is used mainly for flux and reactivity calculations.

FAIM[3] — FAIM is similar to AIM-6, but input information is entered differently. Several additional options are also provided.

ULCER[4] - ULCER is also similar to AIM-6 except that upscattering of neutrons, i.e., gain of neutron energy through collision, is considered.

SNG[5] — SNG is an early one-dimensional transport theory code utilizing up to 20 energy groups and is used mainly for criticality studies. This code has been superseded by DTK.

DTK[6] – DTK is an updated one-dimensional transport theory code which is faster than SNG. The code can utilize as many energy groups as machine capacity will allow. DTK is mainly used for criticality calculations and for examination of effects outside the core, near boundaries, etc.

BAM[7] – BAM computes thermal group constants assuming ability to separate space and energy. The code iterates between an S_4 spatial calculation and a spectrum calculation. BAM is used primarily in cross section studies.

SIZZLE[8] – A multigroup, one-dimensional burnup code based on AIM-6 which uses 16-group flux calculation to weight cross sections, then reduces to 1-6 groups for burnup calculation.

QUICKIE[9] – QUICKIE is a one-region infinite medium, multigroup code used for studying neutron slowing down and thermalization.

HYTRAN[10] – The HYTRAN code is used for the study of diffusion and redistribution of hydrogen within zirconium-uranium hydride fuel elements. The time-dependence of redistribution, reactivity effects accompanying redistribution, and hydrogen pressure in the fuel element gas gap are computed by this code.

HYLO[11] – The HYLO code is employed to calculate hydrogen leakage from SNAP 10A fuel elements. The axial and radial power distribution in the reactor core is employed to determine the power generation in each fuel element. Using the power generation, the code calculates an average temperature for each axial segment (node) of each fuel element and sums the associated hydrogen leakage from each node to obtain the total hydrogen loss. The hydrogen leakage rates are based on 1200°F isothermal permeation rate data[12, 13]

DDK[6] – DDK is a two-dimensional transport theory code used to calculate reactivity effects due to neutron streaming.

B. REACTOR EXPERIMENTS

The calculational methods used in nuclear analyses of the SNAP 10A reactor have been updated and improved by the steady flow of experimental information

from nuclear tests conducted under the SNAP program. The nuclear data has been developed in two general types of tests: (1) tests conducted on reactors operating at design temperature and power and (2) experiments carried out in critical assemblies operating at ambient temperature and essentially zero power. The data obtained from the reactors operating at design conditions is obviously more inclusive than that produced in the critical assemblies since temperature and power-dependent nuclear effects cannot generally be determined in critical assemblies. However, the critical assemblies, which have cost, availability, and flexibility advantages over the operating reactor systems, have contributed significantly to knowledge of nuclear worths, cold clean excess reactivities, drum and reflector characteristics, etc.

Characteristics of the two experimental reactors which have provided data of importance in SNAP 10A reactor design are presented in Table 4. The table shows that these reactors, SER and S2DR, were similar in many respects to the SNAP 10A reactor. The SER was built and operated before the S2DR. It provided the first experimental information on temperature coefficients, power defect and short- and long-term reactivity effects in SNAP reactors. However, the core and fuel dimensions, fuel cladding material, and reflector dimensions specified for SER differed from those proposed later for the SNAP 10A reactor. The S2DR was similar in design to the SNAP 10A reactor; the experimental information developed during the S2DR program was therefore more applicable to SNAP 10A design than was the earlier SER data. The S2DR was in operation between April 1961 and December 1962. Details of SER and S2DR design, operation, and experimental results are discussed in References 14 and 15.

The S10FS-1 ground test reactor also operated for a short period of time at power levels in the vicinity of 0.1 watt. This reactor provided nuclear data which was useful in establishing final fuel loadings for the demonstration and flight systems. Information obtained from the S10FS-1 tests is summarized in Section IV-A.

Three critical assemblies have also contributed considerable information of value to the SNAP 10A program. These critical assemblies were all of the SCA-4 series and include SCA-4C, SCA-4B, and SCA-4A (References 16 and 17). Each of the SCA-4 critical assemblies have employed the same 37 element fuel

TABLE 4

COMPARISON OF EXPERIMENTAL REACTORS WITH SNAP 10A

	SER	S2DR	SNAP 10A
Fuel			
Diameter	1.00 in.	1.25 in.	1.25 in.
Cladding Material	347 SS	Hastelloy-N	Hastelloy-N
N_H	6.0	6.5	6.35
Sm_2O_3 Prepoison	None	~5 mg/in.	8.8 mg/in.
Carbon Additive	None	None	0.15% C
Fuel Material	93% ZrH - 7% U	90% ZrH - 10% U	90% ZrH - 10%U
End Reflector	1-1/2 in. Be	1-1/2 in. BeO	None
Active Fuel Length	10 in.	10 in.	12.25 in.
Reactor			
Operating Power	30 to 50 kw	30 to 50 kw	39.5 kw
No. of Fuel Elements	61	37	37
Coolant	NaK	NaK	NaK
Mass of U^{235}	3.0 kg	3.78 kg	4.75 kg
Grid Plate Material	316 SS	Hastelloy-C	316 SS
Reflector			
Material	Beryllium	Beryllium	Beryllium
Normal Thickness	3.5 in.	2.8 in.	2.0 in.
No. of Active Drums	3	2	2
Total Power Generated	225,000 kwh	272,000 kwh	-

loading. Active fuel length is 12.25 in. and fuel element hydrogen content is $\sim 6.4 \times 10^{22}$ hydrogen atoms/cm^3 fuel. Fuel element end reflectors are not employed.

The SCA-4C critical assembly, which has now been deactivated, provided most of the experimental data utilized in SNAP 10A reactor design. In-core material worths, reactivity effects of fuel and hydrogen, reflector and shim worths, control drum worths, worths of materials and human mockups outside the core, and safety characteristics were experimentally determined in this assembly.

The SCA-4B assembly was used primarily to examine the safety problems associated with water immersion of the SNAP 10A core. The SCA-4B assembly was located within a large water tank, the liquid level of which was varied to simulate complete or partial flooding and/or immersion of the reactor. The reactivity worths of the SNAP 10A shipping sleeve and void filler blocks were measured in SCA-4B. These devices were designed to prevent attainment of criticality during water immersion of the SNAP 10A reactor during a credible accident. Reactivity as a function of internal and external water height, number of elements in the core, and thickness and composition of sleeve and void regions was determined in the SCA-4B assembly.

The SCA-4A critical assembly was designed to be used in connection with the SNAP 2 program. The beryllium reflector for this assembly is of multipiece construction. Mockups of various reflector configurations are therefore possible. The assembly has been employed to determine radial and axial incremental reflector worths, control drum worths, effect of shaping or shaving reflector surfaces, nonstandard geometrical arrangements, etc. Since it was the only critical assembly available during calendar year 1964, it was also utilized for special nuclear studies carried out in connection with the SNAP 10A FS-1, FS-3, FS-4, and FS-5 fuel loadings. The excess reactivity, worth of samarium loading, and worth of hydrogen in each of these cores has been measured in SCA-4A.

C. REACTOR NUCLEAR CHARACTERISTICS

SNAP 10A reactor nuclear analyses can be divided into three general areas: (1) analysis of the reactor parameters, including calculations of cold clean excess reactivity and investigation of the nuclear effects accompanying initial rise to temperature and power; (2) analysis of nuclear effects which occur over reactor lifetime; and (3) analysis of the transient and safety aspects of the reactor, including studies of safety, startup transients, and ultimate shutdown mechanisms. The present report is primarily a description and summary of studies conducted in the first two areas. Details of SNAP 10A safety and transient studies are provided in References 18 and 19. However, nuclear information on which the safety studies are based is summarized in the present document.

The reactivity lifetime changes which occur when the SNAP 10A reactor is brought from the cold clean condition to power and temperature and then operated for 1 year are:

1) Short-Term Reactivity Defects

a) Temperature and Power Defects Associated With Bringing the Cold Reactor Up to Operating Temperature and Power

The reactor temperature defect is produced by a combination of axial fuel expansion, gridplate expansion, and spectral effects. The temperature defect is relatively large in the SNAP 10A reactor. An appreciable fraction of the initial core excess reactivity is required to overcome this defect. The power defect, which is due to departure of the core from isothermal conditions as power is increased, is much smaller than the temperature defect. Reflector temperature changes and reflector movement relative to the core are predicted to produce additional negative reactivity effects during startup.

b) Short-Term Nuclear Effects Which are Completed or Partially Completed Within the 72-hr Active Control Period

These effects include the negative reactivity change accompanying xenon buildup to equilibrium and the negative reactivity change associated with partial completion of hydrogen redistribution within fuel elements.

2) Long-Term Nuclear Changes Which Occur at an Approximately Constant Rate Over the 1-yr Reactor Operating Lifetime

The negative reactivity changes resulting from hydrogen loss, fuel depletion, and fission product accumulation and the positive reactivity contribution occurring as a result of burnout of samarium prepoison are in this category. In addition, that fraction of hydrogen redistribution which occurs after the completion of the 3-day active control period is classified as a long-term effect even though the process is nonlinear and essentially complete within 1-month after startup.

The methods by which the nuclear effects discussed above have been computed are discussed in detail in the following sections. Comparisons with experimental data are provided.

1. Reactivity Coefficients

a. Temperature Coefficients

The overall temperature defect of the SNAP 10A reactor can be computed by multiplying the temperature coefficients associated with the various components of the reactor by the temperature change to which these components are subjected. The overall temperature coefficient represents the sum of several temperature effects. The fuel effect is caused by axial fuel expansion and alterations to the neutron energy spectrum. The upper and lower gridplates each provide separate effects due to radial expansion, and there is also a contribution from the reflector. Both fuel element expansion and NaK expansion cause a decrease in the amount of NaK present in the core, but in-core NaK worth is very low in SNAP 10A and these effects are not significant. The use of fully enriched uranium fuel reduces the Doppler broadening effect to a negligible value; in SNAP reactors this effect may also be neglected. The fuel moderator elements are relatively large and closely spaced so that the reactor core may be assumed to be homogeneous, i.e., no cell effects need by considered.

The temperature coefficients are related by the equation

$$\alpha_{iso} = \alpha_f + \alpha_{UGP} + \alpha_{LGP} + \alpha_R \qquad \ldots(1)$$

where

α_{iso} = total isothermal coefficient of reactivity

α_f = total fuel temperature coefficient

α_{UGP} = upper gridplate temperature coefficient

α_{LGP} = lower gridplate temperature coefficient

α_R = reflector temperature coefficient.

In SNAP 10A nuclear studies, temperature coefficients are usually quoted in units of ¢/°F. Since one dollar of reactivity is equivalent to 0.008 in Δk, one cent of reactivity is equal to 8×10^{-5} in Δk

1) Fuel Element

The fuel temperature coefficient may be divided into two parts: (1) an effect due to the axial expansion of the fuel, and (2) effects due to changes of neutron energy spectrum with temperature. The change in length of the fuel

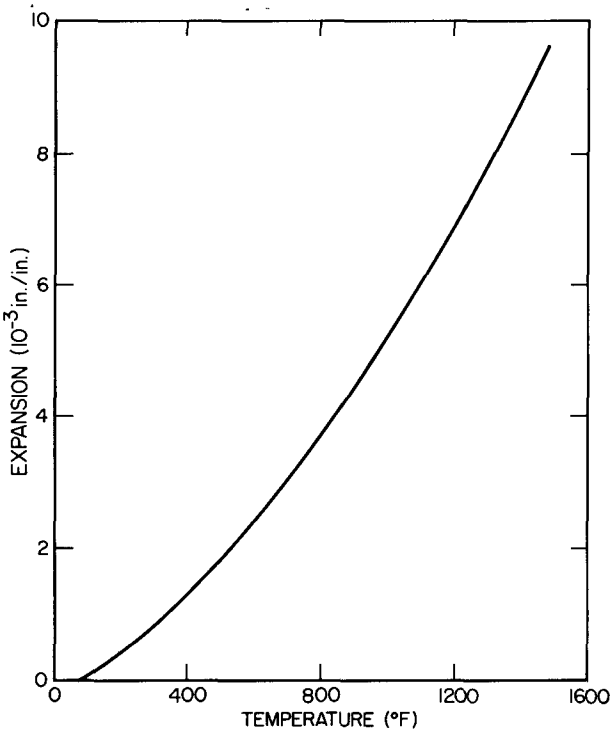

6-12-64 7623-0296

Figure 7. Linear Expansion Coefficient for Uranium-Zirconium Hydride

due to thermal expansion, with the subsequent change in fuel atom densities, results in a change in reactivity with temperature. Since the fuel alloy does not expand linearly with temperature (Figure 7) the expansion coefficient varies with temperature.

Two analyses of reactivity coefficient due to fuel expansion have been completed. Both analyses employed the AIM-6 computer code to determine the reactivity effects due to material atomic density and neutron leakage changes with temperature. The primary difference between the analyses was that Miller, Brehm, and Roberts[20] used group independent bucklings to account for neutron leakage, while Faelten and Swenson[32] employed group and region dependent bucklings in their analyses. The results of both studies are summarized in Table 5.

As the reactor temperature increases, the energy spectrum of the neutrons changes. Calculations of the reactivity effect due to this spectral shift have also been performed by Miller, Brehm, and Roberts and by Faelten and

Swenson. The Miller, Brehm, and Roberts[20] fuel spectral coefficient was calculated by first obtaining temperature-dependent cross sections for the fuel alloy using the neutron thermalization code QUICKIE. The reactivity effect of these cross sections changes was then calculated using the multigroup diffusion theory code ULCER. The method used is described in detail in Reference 20.

The QUICKIE code employs an infinite medium model which may be modified by reading in buckling terms to account for neutron leakage from a finite system, and cross sections weighted over an H-Zr spectrum. The Faelten-Swenson[32] calculation of fuel spectral coefficient was performed using the QUICKIE code with group dependent bucklings. Other assumptions made in the analysis were essentially the same as those of Miller, Brehm, and Roberts.[20] The results of the two analyses were in fair agreement; however, the latter analysis indicates a slightly lower spectral coefficient. The analytical and experimental fuel coefficients are compared in Table 5. Both calculations predict significantly lower total fuel coefficients than were observed in S2DR experiments (Figure 8).[14] The calculations also fail to predict the strong dependence of coefficient on temperature that was observed in S2DR. The S10FS-1 test provided further data on overall isothermal temperature defect. However, it was not possible to accurately separate the defect into individual components.

(2) Gridplate and Reflector Coefficients

The gridplate and reflector temperature coefficients of reactivity result from geometric changes in the reactor core, vessel, and reflector produced by coolant temperature changes. The coefficients result primarily from three effects: (1) changes in grid plate and reactor vessel dimension with coolant temperature, (2) variations in the gap width between the reactor vessel and the reflector as coolant temperatures change and (3) changes in reflector position and density produced by reflector temperature change. The first and second effects follow coolant temperature changes closely and may be lumped together in estimating a "gridplate" coefficient. There is considerable delay time associated with portions of the third effect, i.e., the changes in reflector positions and density as a result of in-core coolant temperature change which produce a "reflector" coefficient. The mechanisms by which the first two effects provide temperature coefficients of reactivity are discussed below.

TABLE 5

COMPARISON OF CALCULATED AND EXPERIMENTAL FUEL TEMPERATURE COEFFICIENTS

	Temperature Range (°F)	α_f(¢/°F)	Codes
Axial expansion (20) contribution	70 - 600 >700	-0.03 -0.04	AIM-6
(32)	70 - 550 700 - 1000	-0.041 -0.049	AIM-6
Spectral (20) contribution	Essentially constant over SNAP 10A temperature range	-0.03	QUICKIE and ULCER
(32)	70 - 300 300 - 700 700 - 1000	-0.024 -0.029 -0.017	QUICKIE
SER isothermal (20) measurement	600	-0.06 to -0.10	
S2DR (14) isothermal measurement	70 - 1200 100 1000	α_f = -0.075 - 0.000057 T (T in °F) -0.081 -0.132	

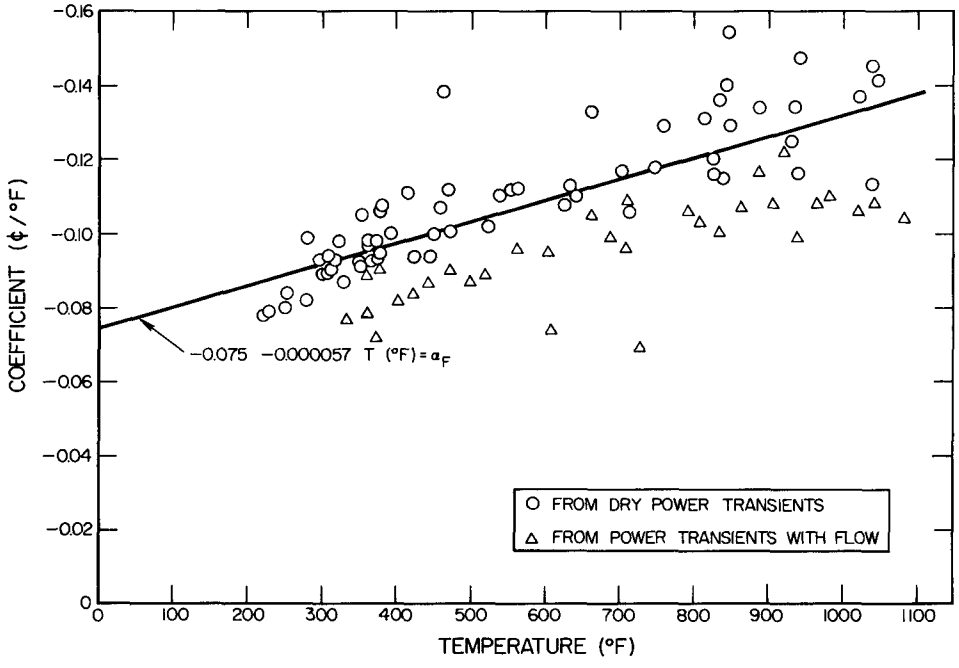

5-26-64 7623-0297

Figure 8. S2DR Experimental Fuel Temperature Coefficient

Grid Plate Coefficient

An increase in isothermal coolant temperature produces simultaneous expansion of the grid plate and reactor vessel. Grid plate radial expansion results in reactivity losses due to reduction of effective fuel density in the core and an increase in axial neutron leakage. The accompanying expansion of the reactor vessel provides a small reactivity gain resulting from an initial reduction in the width of the gap between the reactor vessel and the reflector. The reflector support hinges attached to the bottom of the vessel are also assumed to expand outward simultaneously with the reactor vessel and grid plates. However, the gap opening caused by expansion of the support hinges at the bottom of the reflector does not completely compensate for the reduction in gap width due to vessel expansion, and the overall initial gap reactivity effect is positive.

The previous discussion indicates that the effective upper and lower grid plate coefficients may be unequal due to inequality of the reactor vessel-reflector gap width at the top and bottom of the reflector. In addition, during normal nonisothermal operation at power, the lower grid plate is bathed in coolant at uniform temperature while the upper grid plate is slightly nonisothermal due to radial coolant temperature gradients. Further differences in coefficient result from the fact that the upper grid plate is exposed to a higher absolute temperature than the lower grid plate, and thermal expansion coefficients are therefore slightly different.

An analysis of isothermal grid plate coefficients has been completed using the DTF* code. The simplified analytical model used accounted for grid plate and core vessel radial expansion with accompanying changes in core density and axial neutron leakage. Axial expansion of the reactor core was not considered as this effect is defined as part of the fuel coefficient. Volume fractions and atomic densities were calculated for various gridplate radii corresponding to specific gridplate temperatures between 70 and 1000° F. Density changes and radial motion of both internal and external beryllium reflectors were also considered. The axial neutron leakage effect was computed by iterating between radial and axial DTF calculations until both radial and axial DB^2 (diffusion coefficient times buckling) terms differed by less than 1% from the previous iteration.

*FORTRAN version of the DTK one-dimensional transport theory code.(6)

This calculation was performed for both ambient conditions and 1000°F isothermal conditions. All reactivity calculations for temperatures between ambient and 1000°F employed the ambient condition axial buckling terms.

These calculations were then adjusted for temperature on the basis of the difference observed between grid plate defect for 1000°F calculated using ambient DB^2 terms and the 1000°F defect calculated employing DB^2 terms applicable to the higher temperature.

It was assumed in the initial defect calculations that the gap between the core vessel and reflector remained constant. The core vessel-reflector gap width was then determined for several isothermal reactor temperatures, assuming the reflector temperature to be constant at its initial ambient value (70°F). The reactivity worth of the gap (cents per mil) was calculated and correction terms applied to the initial idealized grid plate coefficients. The results of these calculations are summarized in Table 6. The stainless steel 316

TABLE 6

TEMPERATURE COEFFICIENTS FOR SNAP 10A REACTOR GRID PLATES*

Coolant Temperature (°F)	Grid Plate Temperature Defect Before Gap Correction	Grid Plate Temperature Defect After Gap Correction	Effective Overall† Isothermal Grid Plate Coefficient	Effective Upper Grid Plate Coefficient (¢/°F)	Effective Lower Grid Plate Coefficient (¢/°F)
70-1000	-$1.54	-$1.17	-0.126¢/°F	-0.052	-0.074
900-1000	-$0.18	-$0.14	-0.14¢/°F	-0.060	-0.080

*Grid plate material = stainless steel 316

†Includes changes in grid plate, reactor vessel, and gap width dimensions only. Long-term nuclear effects of changes in reflector density and position are considered part of the reflector coefficient and are discussed later in this section.

linear thermal expansion information on which the grid plate coefficient calculations are based is plotted in Figure 9. Expected isothermal grid plate temperature defect is shown as a function of coolant temperature in Figure 10.

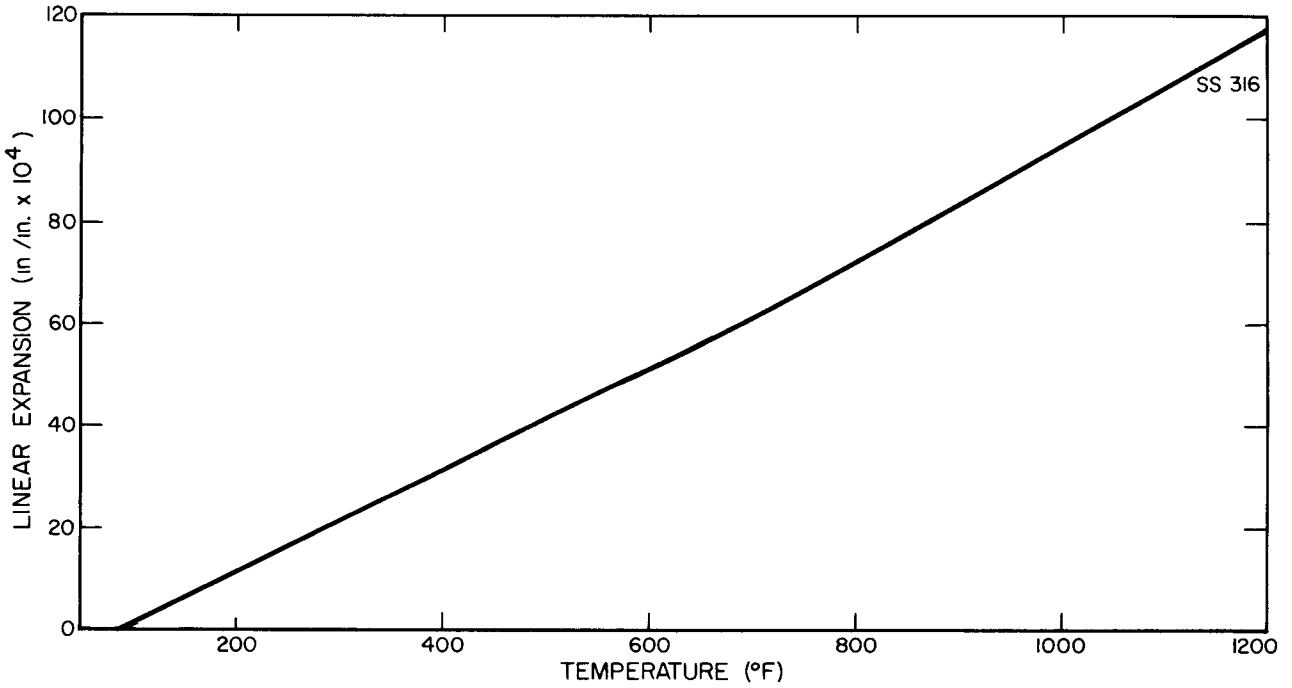

6-12-64 7623-0298

Figure 9. Linear Expansion Coefficient for 316 Stainless Steel

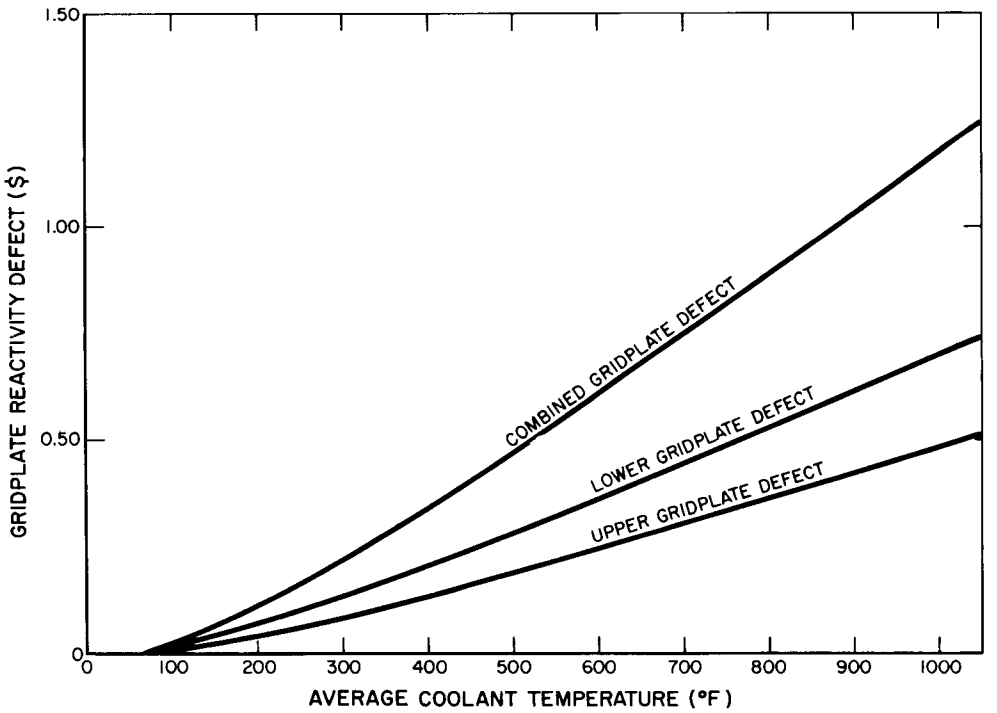

5-26-64 7623-0299

Figure 10. SNAP 10A Isothermal Gridplate Defect vs Average Coolant Temperature

Gridplate coefficients have been determined experimentally in the SER, S2DR, and SCA-4C reactors. The SER transient experiments indicated that the SS-316 upper grid plate coefficient was -0.085¢/°F at 600°F. The measurement was made with coolant flow and analysis of the experiment was carried out by analog simulation. The total overall temperature coefficient obtained was a "best fit" of experimental data. The grid plate coefficient was determined by subtracting the previously measured fuel coefficient from the observed temperature coefficient. Measured and calculated isothermal temperature coefficients are shown in Figure 12.

The SCA-4C top grid plate coefficient was measured by insulating the grid plate from the fuel, isolating the internal reflectors, and then heating the grid plate electrically. The heating was quite rapid so that conduction to the fuel was minimized. Some experimental error was introduced by temperature gradients across the grid plate, and by conduction of heat to the reactor vessel wall. The coefficient for the SS-316 grid plate alone was found to be -0.026¢/°F. This value was then corrected to account for movement of the internal beryllium reflectors, which would have occurred if they had been attached to the grid plate as is the case in an operating reactor. The corrected coefficient was estimated to be -0.034¢/°F.

The methods used in measuring and analyzing the results of S2DR grid plate coefficient experiments are covered thoroughly in Reference 18. Results of S2DR, SER and SCA-4C grid plate experiments are summarized in Table 7. The S2DR reflector was mounted in such a way that the relative

TABLE 7

MEASURED GRID PLATE COEFFICIENTS

S2DR Temperature (°F)	Upper Grid Plate (¢/°F)	Lower Grid Plate (¢/°F)
700	-0.07	-0.062
900	-0.098	-0.066
1000	-0.096	-0.068

SER: SS-316 upper grid plate at 600°F = 0.085¢/°F
SCA-4C: SS-316 upper grid plate at 75 to 570°F = 0.034¢/°F

magnitude of the upper and lower gridplate coefficients is reversed from those calculated for SNAP 10A.

Recent S10FS-1 reactor ground tests did not permit measurement of the grid plate reactivity coefficients although overall coefficients were obtained. The information provided by the tests is summarized in Section II.C.1.c and Section IV.A.

Reflector Coefficient

The reflector defect is defined as the reactivity loss associated with increasing the reflector temperature from ambient to reactor operating level. As previously noted, expansion of the reflectors (which results in an increase in reflector-vessel gap), changes in reflector position, and beryllium density changes are the primary reactivity loss mechanisms. The reflector coefficient is the first derivative of the reflector defect with respect to reflector temperature.

The mechanical coupling of the SNAP 10A reactor and reflector is such that the reactor is expected to be exactly centered with respect to the reflector when both are operating at design conditions. The support hinges at the bottom of the reflector restrain motion, producing unequal coefficients at the top and bottom of the reflector. The effect of changed beryllium density is equal at top and bottom since the reflector operates at essentially isothermal conditions.

The reflector coefficient was calculated as shown below:

$$\alpha_R = \alpha^{Top} + \alpha^{Bottom} + \alpha^{Density}$$

$$\alpha_R \Delta T_R = \frac{r}{2}(E_R \Delta T_R)\beta_{GAP} + \Delta GAP\, \Delta T_R \beta_{GAP} + \alpha^{Density} \Delta T_R$$

$$\alpha_R \approx -0.042 ¢/°F \text{ between } T_R = 70°F \text{ and } 800°F$$

where:

α_R = reflector coefficient of reactivity (¢/°F)

E_R = reflector thermal expansion coefficient (in./in. °F)

ΔT_R = reflector temperature change (°F)

β_{GAP} = worth of reflector-vessel gap in cents per inch = -0.0013¢/in.

$\alpha^{Density}$ = reflector coefficient of reactivity due to change in beryllium density resulting from temperature changes (¢/°F)

r = average radius of reactor vessel-reflector gap (inches)

and where Δgap (inches/°F) is defined by the following equation:

$$2\pi R\Delta GAP = \int_{-4.513}^{-4.51} \left\{ \left[R(1 + E_R\Delta T_R) \right]^2 - \left[\chi - AE_R\Delta T_R \right]^2 \right\}^{1/2} d\chi$$

$$+ \int_{-4.51}^{-4.44} \left(\left\{ \left[R(1 + E_R\Delta T_R) \right]^2 - \left[\chi - AE_R\Delta T_R \right]^2 \right\}^{1/2} - \left\{ R^2 - \chi^2 \right\}^{1/2} \right) d\chi$$

$$+ \int_{-4.44}^{+0.49} \left(\left\{ R^2 - \chi^2 \right\}^{1/2} - \left\{ \left[R(1 + E_R\Delta T_R) \right]^2 - \left[\chi - AE_R\Delta T_R \right]^2 \right\}^{1/2} \right) d\chi$$

$$+ \int_{+0.49}^{+4.51} \left(\left\{ \left[R(1 + E_R\Delta T_R) \right]^2 - \left[\chi - AE_R\Delta T_R \right]^2 \right\}^{1/2} - \left\{ R^2 - \chi^2 \right\}^{1/2} \right) d\chi$$

$$+ \int_{+4.51}^{+4.536} \left[R(1 + E_R\Delta T_R) \right]^2 - \left[\chi - AE_R\Delta T_R \right]^2 \Big\}^{1/2} d\chi$$

Where R is the radial distance from the center-line of the reactor vessel to the center point of the fixed reflector hinge in inches; A is the x-coordinate of R in inches; and $E_R\Delta T_R$ is the linear growth of the reflector halves away from the hinge points in inches per inch. This definition of ΔGap is necessary in order to describe the complex motion of the reflector relative to the bottom of the reactor. The lower portion of the reflector is fixed in position at one point by the reflector support hinge, so that all reflector expansion occurs relative to that point.

The reflector-vessel gap change calculation indicates a top-of-reflector coefficient (α^{Top}) of -0.020¢/°F of reflector temperature. The corresponding bottom-of-reflector coefficient (α^{Bottom}) is -0.011¢/°F of reflector temperature. The DTK code was employed to calculate the reactivity effect due to reflector density changes. The calculated reactivity coefficient ($\alpha^{Density}$) due to density changes was -0.011¢/°F of reflector temperature.

The average total reflector coefficient (α_R) up to 800°F reflector temperature is calculated to be -0.042¢/°F, with the top of the reflector contributing -0.026¢/°F and the lower portion -0.016¢/°F.

The width of the vessel-reflector gap has been calculated as a function of time after reaching critical. Figure 11 shows that the average cap width is reduced from the initial cold value of 65 mils to about 43 mils by the time the approach to power is completed. The gap then widens to about 55 mils as the reflector approaches its equilibrium temperature.

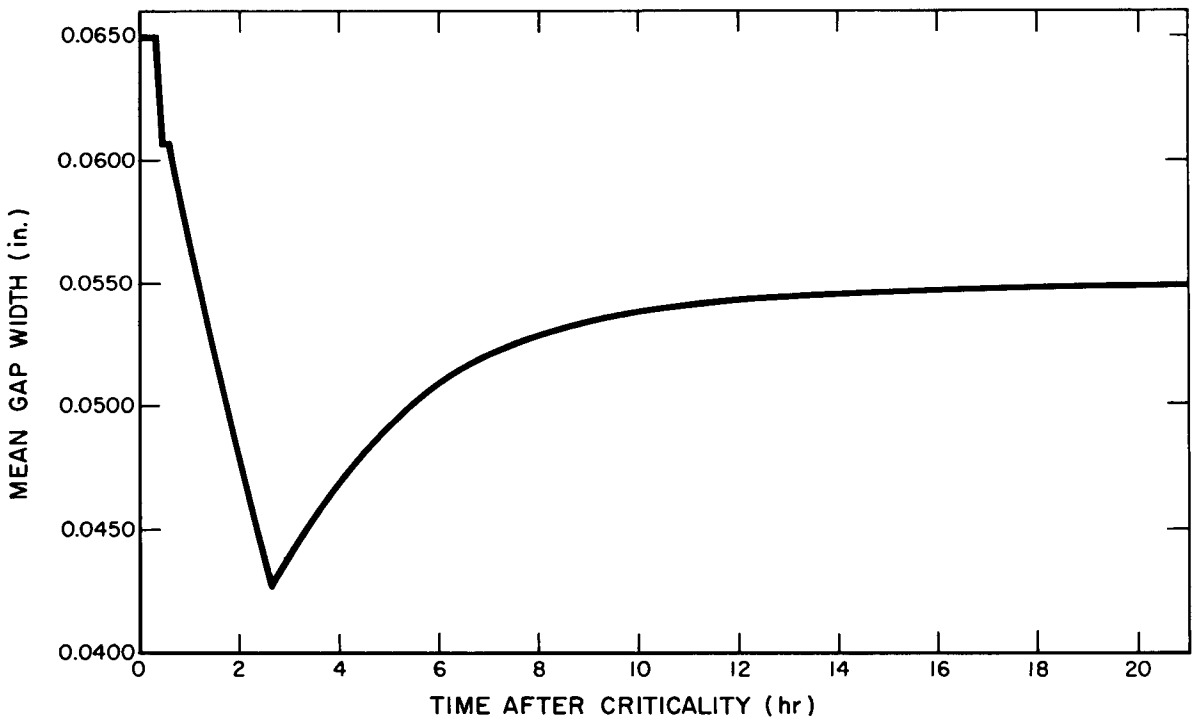

Figure 11. SNAP 10A Reflector-Vessel Gap Width vs Time After Criticality

The reflector temperature coefficient of SNAP 10A was measured during the low-power nuclear test sequence. The measured total reflector coefficients were -0.025¢/°F and -0.043¢/°F at reflector temperatures of 200°F and 550°F respectively. The agreement between analysis and experimental reflector coefficient changed erratically during the course of the experiment. Thermal reference tests to be performed on the demonstration test reactor and flight systems will provide additional data on reflector effects. Early analysis of SNAP 10A reflector coefficient at startup, most of which is now obsolete, is discussed in Reference 22.

b. Power Coefficient

In addition to the isothermal temperature coefficients discussed, there is a reactivity effect associated with changes in reactor power. The coefficient results from increasing departure of reactor components from isothermal temperature conditions as power is increased. The power coefficient of the SNAP reactors (usually expressed in ¢/kw) is related to the individual component temperature coefficients by the following expression:

$$\alpha_P = \left[\frac{1}{2}\frac{(\Delta T_{in} + \Delta T_{out})}{\Delta P} + \frac{1}{UA}\right]\alpha_F$$

$$+ \frac{\Delta T_{in}}{\Delta P}\alpha_{LGP} + \frac{\Delta T_{out}}{\Delta P}\alpha_{UGP} + \frac{\Delta T_R}{\Delta P}\alpha_R \qquad \ldots(2)$$

where:

ΔT_{in} = Change in coolant inlet temperature with power

ΔT_{out} = Change in coolant outlet temperature with power

ΔT_R = Reflector temperature change with power

ΔP = Power change associated with the above temperature changes

UA = Average heat transfer coefficient times heat transfer area

α_F = Fuel temperature coefficient

α_P = Power coefficient

α_{LGP} = Lower gridplate temperature coefficient

α_{UGP} = Upper gridplate temperature coefficient

α_R = Reflector temperature coefficient.

Attempts to correlate analytical and experimental values of power coefficient have not been completely successful. The cause of the lack of correlation is the considerable uncertainty in the individual temperature coefficients and in the calculation of the average overall thermal resistance (1/UA) between the fuel rod and coolant. Most of the uncertainty in the 1/UA value results from uncertainties as to the quantity of inert gas, hydrogen and/or air in the gap between the fuel rod and cladding.

Analysis of the SER and S2DR experimental results indicates that — assuming constant inlet and outlet temperature and varying flow — the average power coefficient was ~ -0.4¢/kw for those systems.

Since the composition of the gas in the SNAP 10A fuel element gap is quite well known, it has been possible to calculate 1/UA values with much more accuracy than was possible for the SER and S2DR fuel elements. Analysis of the flight system fuel elements indicates that the power coefficient, assuming constant ΔT across the core and variable coolant flow rate, is -0.17¢/kw using the S2DR fuel coefficient and -0.09¢/kw using the Faelten-Swenson fuel coefficient.

2. Reactivity-Lifetime Effects

During the 72-hr active control period which includes and follows reactor startup, reactivity losses are compensated by insertion of control drums. Knowledge of the magnitude of the reactivity losses which occur during the first 72 hr of operation is necessary to assure that sufficient active control (drum rotation) is available throughout this period. The short-term reactivity losses which must be considered are: (a) temperature defect, (b) power defect, (c) xenon accumulation, and (d) hydrogen redistribution, which reaches 40 to 60% of completion during the active control period.

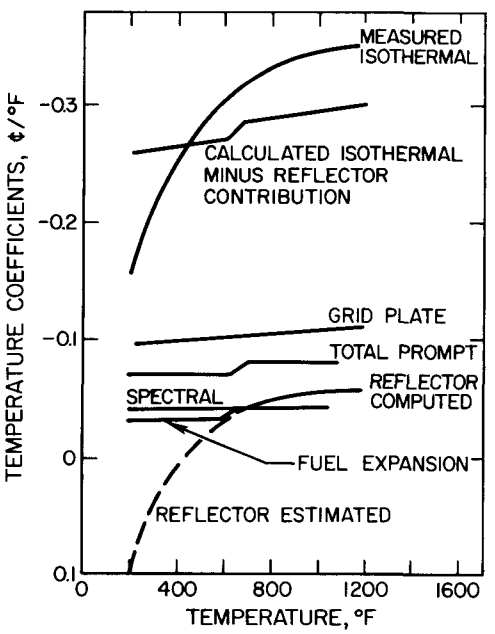

5-26-64 7623-0300

Figure 12. Isothermal Temperature Coefficients in the SER Reactor

Short term reactivity defects are summarized in Table 8. The defects shown all occur during the approach to power and the 64 hour active control period after reaching full power. It requires 6.1 hr to achieve criticality by inserting control drums from the full-out position to approximately 62° from full-in. The approach to power then begins. A small power transient is experienced shortly after criticality is reached. The power transient is described in Section III.C.3.a.

The reactivity defects expected during the approach to power were calculated as a function of time and summed to obtain the startup defect. The defects expected during the remainder of the active control period were also calculated as a function of time. The predicted startup and control period defects are shown in Figure 13. Xenon and hydrogen redistribution defects, which are included in the total defect, are also shown as functions of time. The control drum position, when full power is reached, is expected to be 30.3° from full-in.

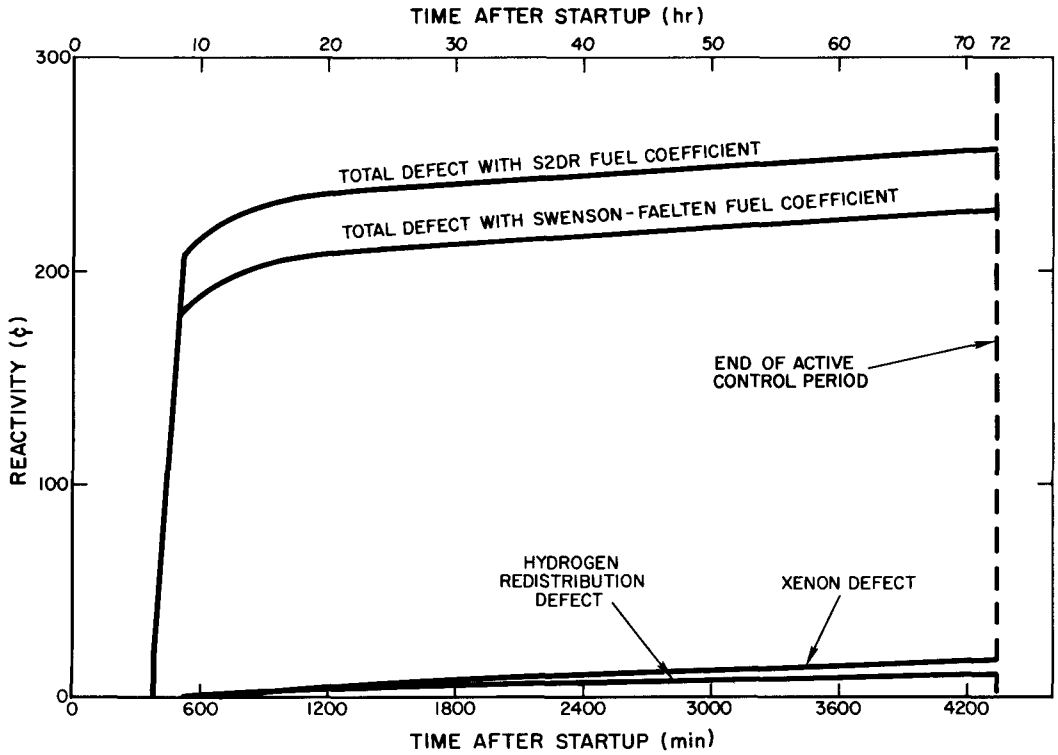

Figure 13. Predicted SNAP 10A Reactivity Defects vs Time

TABLE 8

SHORT-TERM REACTIVITY EFFECTS
(72-hr startup period)

	With Faelten-Swenson Fuel Coefficient	With S2DR Fuel Coefficient
Predicted Approach-to-Power Defects (¢)		
Reactor temperature	168.8	194.5
Reflector temperature	6.5	6.5
Hydrogen redistribution	0.3	0.3
Power	3.7	7.1
Xenon	~0.0	~0.0
Total	179.3	208.4
Predicted Active Control Period Defects (¢)		
Reflector temperature	21.7	
Hydrogen redistribution	10.7	
Xenon	17.2	
Total	49.6	
Predicted Total Startup Defect (¢)		
Approach-to-power	179.3	208.4
Active control period	49.6	49.6
Total	228.9	258.0
Available Excess Reactivity = $3.00 ± $0.10		
Contingency	$0.71	$0.42

The control drum position at the end of the active control period, based on use of the S2DR fuel coefficient, is predicted to be 20° ±7°. The uncertainty in final control drum position is primarily due to uncertainties in prediction of the magnitude and rate of hydrogen redistribution. The temperature defect predicted using the S2DR fuel coefficient is in good agreement with the defect measured in S10FS-1. (See Table 18, Section IV.A).

Fast neutron doses at the instrument compartment are quite dependent on the position of the control drums during normal static control operation. Early nuclear analysis predicted a final control drum position of 22° from full-in; all shielding analyses have been performed for that condition.[34] An actual final drum position closer to full-in than 22° would significantly reduce the fast neutron dose during the year of static control operation.

Maintenance of a stable power level and operating temperature for the remainder of reactor lifetime (1 yr) is accomplished by static control. The reactivity effects occurring during this time are due to hydrogen leakage, the remainder of the hydrogen redistribution (essentially completed in 1 month), fuel depletion through burnup, and fission product accumulation. To counteract these losses in reactivity, a predetermined amount of samarium is loaded into the core. As the samarium prepoison burns up, positive reactivity is made available to compensate for reactivity losses and to maintain the desired operating conditions.

Long-term reactivity effects are summarized in Table 9. A brief discussion of both long- and short-term effects is presented in the following sections. The "contingency" shown in Table 8, is needed to overcome any reactivity uncertainties which become apparent during the active control period. The uncertainty in short-term reactivity losses is due to experimental and/or calculation limitations. A brief discussion of these reactivity effects is presented in the following sections.

a. Short-Term Reactivity Effects

Temperature Defect

The reactivity defect associated with increase of the reactor coolant temperature from room temperature to operating temperature is the largest

TABLE 9

LONG-TERM REACTIVITY EFFECTS
(remainder of reactor life – 1 yr)

	Nuclear Effect ($)
Hydrogen redistribution	-0.11 ± 0.06*
Hydrogen leakage	-0.03 ± 0.015
Fuel burnup and fission product accumulation	-0.12 ± 0.02
Samarium prepoison	+0.18 ± 0.04†
Net loss (1 yr)	-0.08 ± 0.13

*Estimated portion of total which occurs following the first 72 hr.
†8.8 mg/in. Sm_2O_3

reactivity loss which must be overcome during reactor lifetime. The reasons for the reactivity loss are discussed in Section IV-C-1-b. The total reactivity loss, or temperature defect, was determined to be approximately $1.95, as discussed in the previous sections.

Power Defect

The reactivity defect associated with a change in reactor power has been described in Section IV-C-1-b. The power defect was determined by multiplication of the power level change by the estimated power coefficient.

Hydrogen Redistribution

Hydrogen redistribution results from fuel rod axial temperature gradient with diffusion of hydrogen from hot regions to those portions of the fuel rod operating at lower temperatures. Hydrogen diffusion in SNAP 10A was calculated using the HYTRAN code.[10] The basic equation used by the code in describing the transfer of hydrogen within a cylindrical fuel rod is,

$$J = - D\left(\frac{\partial N}{\partial r}\right) - D\left(\frac{NQ^*}{RT^2}\right)\left(\frac{\partial T}{\partial r}\right) \quad , \qquad \ldots(4)$$

where,

J = hydrogen flux (moles H_2/cm^2 - sec)

D = diffusion coefficient for movement of H_2 through fuel alloy (cm^2/sec)

N = hydrogen concentration in fuel (H atoms x $10^{22}/cm^3$)

r = fuel rod radius (cm)

Q^* = heat of transport = 1270 cal/mole

T = absolute temperature (°K)

R = gas constant = 1.987 cal/mole -°K

It should be noted that the hydrogen diffusion rate varies inversely with the square of absolute temperature. Therefore, with other parameters fixed, a greater reactivity loss due to hydrogen redistribution would be encountered at lower temperatures than at higher temperatures. This effect is shown in Figure 14. Axial migration of hydrogen within the fuel rod is neglected in the HYTRAN calculation on the basis of the fact that it takes approximately 20 times longer for a hydrogen atom to traverse the axial length of the rod than to migrate radially. Following migration, hydrogen is assumed to be transported along the rod as a gas contained within the fuel-cladding gap. The HYTRAN code also assumes that there is no leakage of hydrogen through the ceramic hydrogen barrier and cladding during the redistribution transient.

The total reactivity loss due to hydrogen redistribution in SNAP 10A was calculated to be -$0.21. The time required to complete hydrogen redistribution was also calculated with HYTRAN. Results of the HYTRAN calculation indicate that redistribution should be completed during the first month of operation. It is estimated that $0.11, or ~50% of the total reactivity change associated with hydrogen redistribution, occurs within the first 72 hr after startup.

Firm experimental data on hydrogen redistribution with which the HYTRAN calculations may be compared are not available at present. From the preliminary information reported in Reference 14, however, it appears that the HYTRAN code computes the magnitude of the reactivity change accompanying redistribution correctly, but tends to underestimate the time required for completion of redistribution.

Xenon Equilibrium

Because of its large thermal absorption cross section ($> 3 \times 10^6$ barns), xenon-135 is the most important fission product from a reactivity standpoint. Xenon-135 is formed primarily by the radioactive decay of tellurium-135 as shown in the following decay chain: $Te^{135} \xrightarrow{1m} I^{135} \xrightarrow{6.7h} Xe^{135} \xrightarrow{9.2h} Cs^{135} \xrightarrow{2.1 \times 10^6 y} Ba^{135}$. Since the half life of tellurium-135 is only $\sim$1 minute, the analysis is somewhat simplified by assuming that iodine-135 is produced directly from fission. The concentration of iodine at any time is given by the following equation:

$$I(T) = \frac{\gamma_I \Sigma_f \varphi}{\lambda_I + \sigma_I \varphi}\left(1 - e^{-\lambda_I T}\right) + I(O)e^{-\lambda_I T} \quad , \qquad \ldots(5)$$

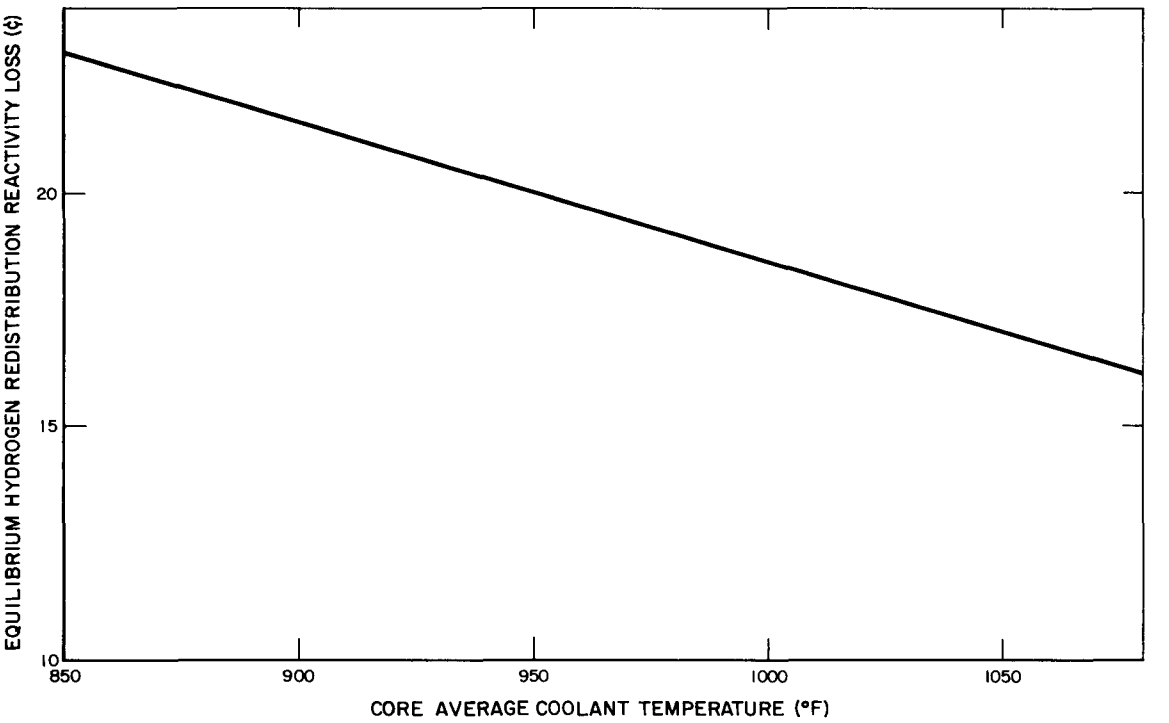

6-12-64 7623-0301

Figure 14. SNAP 10A Hydrogen Redistribution (P = 41.2 kwt)

where,

$I(O)$ = initial iodine concentration $(\frac{atom}{cc})$

$I(T)$ = iodine concentration after time T

T = time (sec)

γ_I = iodine yield from fission $(\frac{atom}{fission})$

λ_I = iodine decay constant (sec^{-1})

σ_I = iodine neutron absorption cross section (barns)

Σ_f = macroscopic U^{235} fission cross section

φ = average thermal neutron flux during time T.

Since σ_I is small compared to λ_I, and $e^{-\lambda_I T}$ goes to zero for large values of T, the equilibrium concentration of iodine is essentially:

$$I_o = \frac{\gamma_I \Sigma_f \varphi}{\lambda_I}$$

where, I_o = equilibrium iodine concentration.

The equilibrium xenon concentration is then given by,

$$X_o = \frac{\lambda_I I_o + \gamma_X \Sigma_f \varphi}{\lambda_X + \sigma_X \varphi} = \frac{(\gamma_I + \gamma_X)\Sigma_f \varphi}{\lambda_X + \sigma_X \varphi} \quad , \qquad \ldots(6)$$

where, X_o = equilibrium xenon concentration and the symbol X is used to denote xenon in previously defined symbols.

The reactivity loss associated with buildup to equilibrium concentration of xenon was derived from xenon transient measurements made in the S2DR. The reactor power was increased from zero to 30.5 kw and then decreased from 30.5 kw to zero. The xenon reactivity defect associated with operation at 30.5 kw was 13.4¢. Since this value is proportional to reactor power, the xenon

defect may also be expressed as -0.41¢/kw. For the SNAP 10A reactor operating at 39.5 kw the xenon defect is then -$0.17. Approximately 99% of the equilibrium xenon concentration is reached within the 72-hr active control period. The time dependence of xenon buildup, calculated using the SIZZLE code, is illustrated in Figure 15.

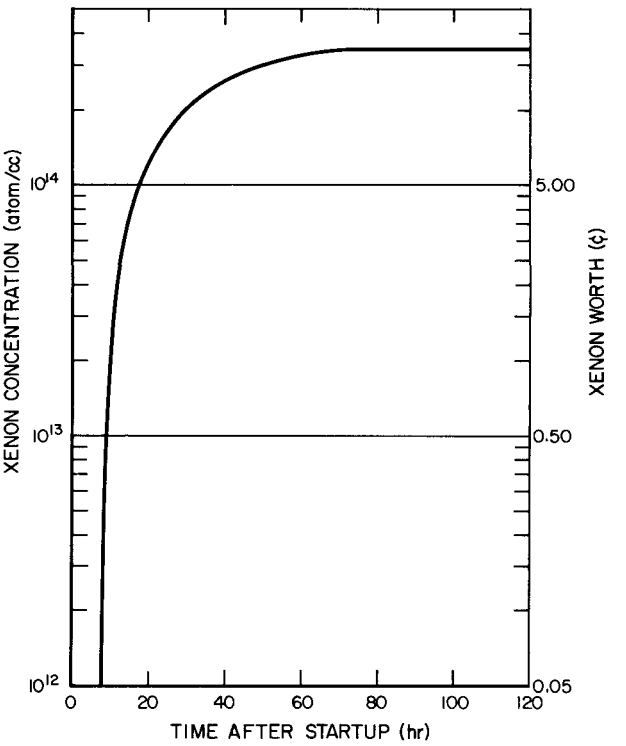

Figure 15. SNAP 10A Xenon Buildup

Equilibrium xenon calculations have been made using the ZOOM code[23] for both the S2DR and SER reactors. Calculations are not in good agreement with the S2DR measured value, but are in fair agreement with the SER measurement. The calculations indicated a 30¢ defect for SER and 33¢ for S2DR at 50 kw,[24] while the measured value for SER was 39¢ at 53 kw. The measured S2DR xenon coefficient of -0.41¢/kw is assumed to be more accurate than the calculated value because some of the cross sections that were used in the ZOOM code calculation are now considered erroneous.

b. Long-Term Reactivity Effects

SNAP 10A long-term reactivity effects are summarized in Table 9. The hydrogen redistribution reactivity loss shown in the table is based on HYTRAN code estimates of the fraction of hydrogen redistribution which occurs after the active control period has been completed. The remaining long-term effects are nearly linear with time during the 1-yr operating period. These effects are discussed in the following sections.

Fuel Burnup and Fission Product Accumulation

The number of fuel atoms fissioned during a year of continuous operation at design power may be calculated readily from the energy released per fission. The calculated total energy release from fission is about 205 Mev

of which about 190 Mev is absorbed in the reactor core, coolant, and structure. Fission product accumulation may be calculated from the operating power level and the yield of various fission product isotopes.

Using the AIM-6 code, the worth of uranium-235 in the SNAP 10A reactor has been calculated to be 9.1¢ per % change in U^{235} concentration. The fraction of fuel burned in 1 yr is calculated to be ~0.32 wt % of the U^{235} initially present; therefore, the reactivity loss due to burnup is approximately 2.9¢. There is some uncertainty in this calculation due to uncertainties in energy release per fission, calculated worth of uranium-235, and the average power level used for the calculation. However, since the total reactivity loss due to fuel burnup is small, great calculational accuracy is not required.

The reactivity loss due to fission product accumulation has been calculated by several methods. The calculation of fission product poisoning is characterized by considerable uncertainty due to the large number of isotopes which must be considered. Only the slowly saturating and nonsaturating fission products are considered here; the important fission product isotopes, xenon, and samarium are discussed separately in other sections of this report.

A rough calculation of reactivity loss was made using the method outlined in Reference 25. A cross section of 60 barns per fission was used in the one-energy-group calculation. The calculated result of ~-2¢ for fission product poisoning during one year of operation probably represents a lower limit for fission product worth. A second method used in calculating fission product defect was the extrapolation of the ORNL data (Reference 26) to the SNAP 10A reactor power level. This method indicates about a -5¢ reactivity effect over one year of operation.

Cross sections for fission products, weighted over a zirconium hydride spectrum, have recently been prepared for use with the SIZZLE code. The revised cross sections are shown in Table 10. A 6-energy-group SIZZLE calculation of fission product poisoning employing these cross sections indicates a 1-yr fission product defect of -9.0¢. The SIZZLE calculation is believed to be the most accurate estimate of the SNAP 10A fission product defect which has been made to date. Using the SIZZLE results, the total one-year reactivity defect accompanying fission product accumulation and fuel burnup is estimated to be -12¢.

TABLE 10

SIXTEEN GROUP, GROSS FISSION PRODUCT ABSORPTION CROSS SECTIONS*
(weighted over zirconium hydride spectrum)

Energy Group	Energy Range	σ_a (barns/fission)
1	10 → 3 Mev	0
2	3 → 1.4	$1.79\ (10)^{-2}$
3	1.4 → 0.9	$6.56\ (10)^{-2}$
4	0.9 → 0.4	$9.77\ (10)^{-2}$
5	0.4 → 0.1	10^{-1}
6	0.1 Mev → 17 kev	$1.62\ (10)^{-1}$
7	17 → 3	$6.34\ (10)^{-1}$
8	3 → 0.55	2.34
9	0.55 kev → 100 ev	7.24
10	100 → 30	29.3
11	30 → 10	22.8
12	10 → 3	67.3
13	3 → 1	35.2
14	1 → 0.4	10.0
15	0.4 → 0.1	20.0
16	0.1 → (thermal)	60.0

*Xenon and samarium not included.

Hydrogen Leakage

Hydrogen leakage from the fuel rod and through the cladding to the coolant occurs continually during normal reactor operation. The migration of hydrogen from the fuel rod to the gap region has been discussed in III-C-2-a. The rate at which hydrogen permeates through the cladding is dependent on the absolute cladding temperature and the hydrogen pressure attained in the gas gap between the fuel rod and the cladding. Hydrogen gap pressure is determined by the dissociation pressure of the uranium-zirconium-hydride fuel alloy. Dissociation pressure is, in turn, a function of fuel temperature distributions, H-Zr ratio, and fuel additive concentration (see Figure 16).[33] In the nominal SNAP 10A reactor, all of these fuel characteristics are fixed.

Hydrogen permeation through the uncoated 15-mil-thick Hastelloy-N cladding tube would be excessive; therefore, a ceramic hydrogen permeation barrier coating has been applied to the interior surface of the SNAP 10A cladding tubes. The ceramic coating was also applied to a cup which fitted over the end of the fuel rod and completed the barrier when blended to the coating on the cladding tube wall.

When it proved difficult to calculate SNAP 10A hydrogen leakage with a theoretical model, an empirical method was developed (Reference 12). The empirical model for calculating hydrogen loss was based on experimental isothermal (uniform temperature) leak rate measurements made on about 50 SNAP 10A fuel elements. The measured isothermal element leak rate (φ_e) was assumed to be the summation of leakage due to diffusion through the permeation barrier (φ_{cl}) and leakage through microscopic cracks and other defects in the ceramic (φ_D). The fuel elements which had the lowest measured leak rate were assigned zero leakage due to barrier defects. Hydrogen loss through these "perfect" barriers is described by the following equation:

$$\varphi_{cl} = \frac{K_{cl} P T^{5/2} e^{-(28160/T)}}{T^{5/2} + 8.432 \times 10^{13} P e^{-(28160/T)}} \qquad \ldots(7)$$

where,

φ_{cl} = Hydrogen permeation rate through cladding, cc(STP)/hr

K_{cl} = Proportionality constant for use in the above equation

P = Hydrogen dissociation pressure (atmospheres)

T = Average absolute cladding temperature (°R)

Since $\varphi_{cl} = \varphi_e$ for the lowest leak rate elements, K_{cl} was readily determined from the experimental data.

The hydrogen leakage rate from the "imperfect" elements was described as $\varphi_e = \varphi_{cl} + \varphi_D$, where $\varphi_D = K_D \sqrt{P}\, e^{-(12760/T)}$. The proportionality constant K_D was then calculated using the measured isothermal leak rate data for nonperfect elements. At normal SNAP 10A operating conditions φ_D represents 90% of the total hydrogen leakage rate.

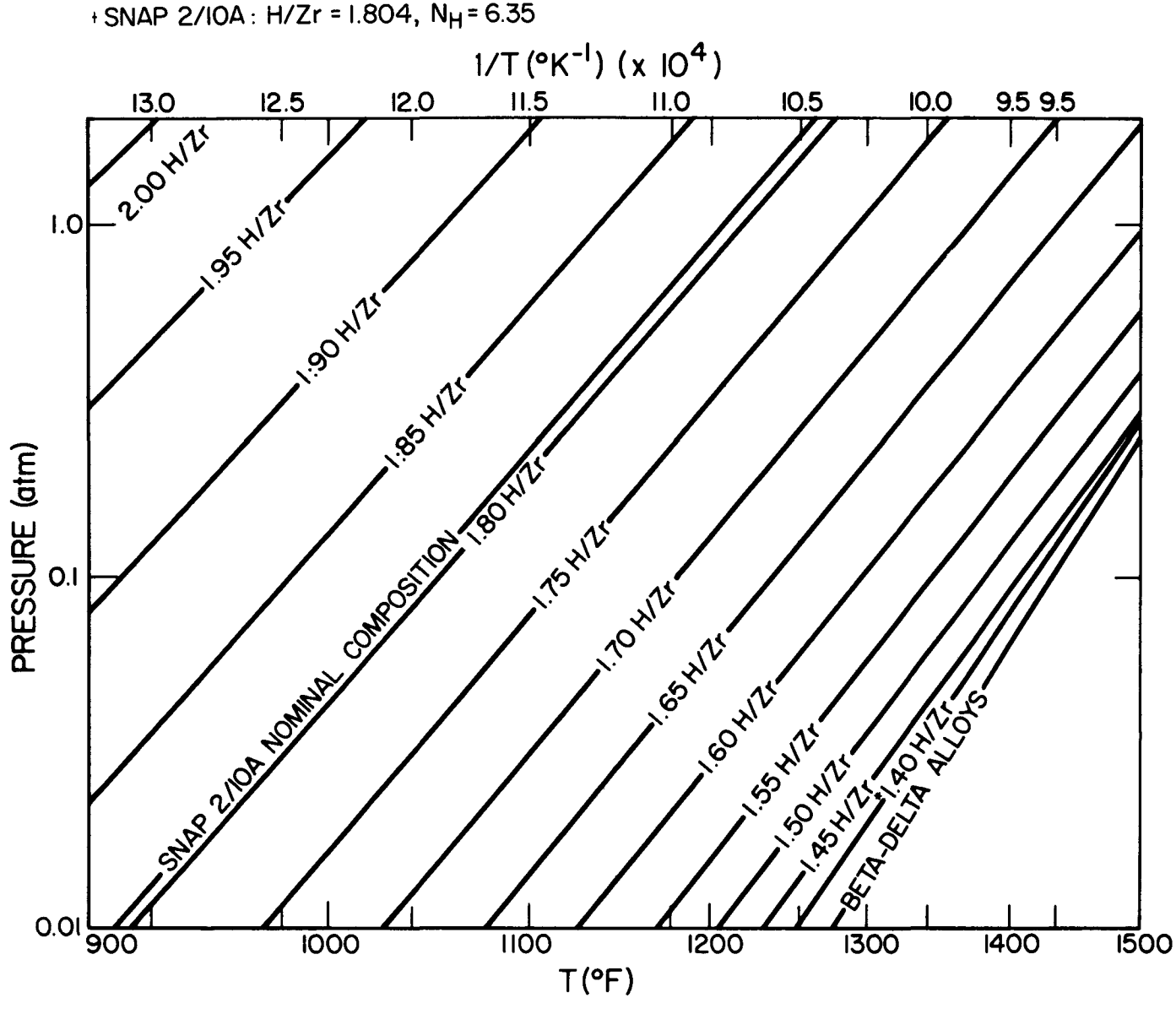

6-24-63 7623-0302

Figure 16. Dissociation Pressures for 0.15 wt % Carbon-Modified SNAP 10A Fuel[33]

A digital computer code called HYLO has been written to calculate hydrogen loss in an operating reactor.[11] Radial and axial temperature distributions in the reactor are calculated and the equilibrium hydrogen pressure in the fuel element gap is computed. Hydrogen leakage from 10 axial nodes of each element is calculated and summed over the 37-element core. The constant K_D was calculated for typical SNAP 10A fuel elements as 1.455×10^6.[13] The constant K_D was calculated for each of the individual fuel elements on which data were available, and an average value was used in the HYLO code.

HYLO computer code analysis of the SNAP 10A reactor indicates that an average hydrogen leak rate of 0.015 cc (STP)/hr-element will be encountered at nominal operating conditions. Assuming that hydrogen which escapes from the fuel element is lost from the reactor, the reactivity effect of hydrogen leakage was calculated by determination of the total hydrogen loss in 1 yr and calculation of the associated change in average fuel N_H (hydrogen concentration). The reactivity effect of hydrogen loss was then determined from the worth of hydrogen (~\$1.00/0.1 N_H unit) to be approximately -3¢/yr at nominal SNAP 10A conditions.

Samarium Prepoison

The long-term reactivity losses discussed in previous sections are partially counteracted by the reactivity gain resulting from burnout of samarium prepoison. The prepoison consists of natural samarium oxide which is mixed with the ceramic hydrogen barrier material before application to the cladding tubes.

Samarium-149 is a highly absorbing (~70,000 barn thermal absorption cross section) stable isotope which is the end product of the following fission product decay chain:

$$Nd^{149} \xrightarrow{1.8h} Pm^{149} \xrightarrow{53h} Sm^{149}$$

Since neodymium-149 has a relatively short half-life, it is assumed that Pm^{149} is formed directly from fission.

Samarium-149 is a saturating fission product which reaches ~90% of its equilibrium concentration after 7-yr of full-power operation at SNAP 10A conditions. The saturation concentration of Sm^{149} may be calculated from the equation:

$$Sm_{eq} = \frac{\Sigma_f}{\overline{\sigma}_{Sm}}\left[\frac{\lambda_{Pm}\gamma_{Pm} + \lambda_{Pm}\gamma_{Sm} + \gamma_{Sm}\overline{\sigma}_{Pm}\varphi}{\lambda_{Pm} + \sigma_{Pm}\varphi}\right] , \qquad ...(8)$$

which reduces to the following equation if the direct samarium-149 yield from fission (γ_{Sm}) and the average promethium absorption cross section ($\overline{\sigma}_{Pm}$) are considered to be negligible.

$$Sm_{eq} = \frac{\gamma_{Pm}\Sigma_f}{\overline{\sigma}_{Sm}} , \qquad ...(9)$$

where,

Sm_{eq} = Equilibrium Sm^{149} concentration

γ_{Pm} = Fission product yield of Pm^{149}

Σ_f = SNAP 10A average, effective macroscopic U^{235} fission cross section

$\overline{\sigma}_{Sm}$ = SNAP 10A average, effective, samarium cross section

Simultaneous with the accumulation of fission product samarium, the samarium-149, which comprises 13.8% of the natural samarium prepoison, is burned out by the reactor neutron flux. By loading prepoison in excess of the reactor equilibrium concentration, it is possible to obtain an effective increase in reactivity as the surplus samarium burns out. The net change in samarium-149 atomic density with time may be calculated with the following equation,

$$Sm(T) = Sm_{eq}\left(1 - e^{\lambda_{SB}T}\right) + Sm(o)e^{-\lambda_{SB}T} , \qquad ...(10)$$

where

Sm (T) = concentration of Sm^{149} at time T

Sm (o) = initial (prepoison) Sm^{149} concentration

Sm_{eq} = equilibrium Sm^{149} concentration

and

$$\lambda_{SB} = \int^{E} \varphi(E)\,\sigma_{Sm}(E)dE = \text{samarium burnup constant}$$

Samarium cross sections from the ULCER library were weighted over a ZrH spectrum using the QUICKIE code, and the reactivity worth of changes in samarium concentration was calculated using the DTK transport theory code.

The reactivity worth of the equilibrium samarium concentration was calculated to be ~$1.09. The initial worth of an 8.0 mg/inch loading of Sm_2O_3 has been determined by calculation and experiment to be ~$1.50. The Sm_2O_3 loading has recently been raised from 8.0 mg/inch to an effective value of 8.8 mg/in. of fuel element by increasing the samarium oxide content of 3 of the 37 elements to 16.0 mg/inch. Correcting for self-shielding and flux depression effects, the initial worth of the revised prepoison loading is predicted to be $1.64 ± 10%. The calculated reactivity gain resulting from this prepoison loading, over 1-yr of operation, is expected to be $0.18 ± 0.04. Figure 17 shows the expected reactivity gain due to prepoison burnout, as a function of initial samarium loading, during 1-yr of continuous SNAP 10A operation at 39.5 kw.

3. Startup and Control

The SNAP 10A reactor has been designed to undergo a simple, effective startup procedure which will minimize the possibility of damage to the fuel elements or reactor. The reactor control system is actuated by ground command after a satisfactory orbit has been established. The two coarse control drums are snapped-in upon actuation of the control system. At the same time, an automatic controller and timer system begins stepwise inward rotation of the two fine control drums at the rate of 1/2° every 150 sec, equivalent to a maximum reactivity insertion rate of 3.3¢/150 sec. Control drum insertion continues until the temperature sensors at the core outlet indicate that the coolant temperature setpoint (1010°F) has been exceeded. The controller is automatically deactivated when the coolant temperature rises above the setpoint and is activated (resumes stepwise reactivity insertions) when the coolant temperature drops below 1010°F.

The automatic controller will be turned off by a ground control signal after three days of active control. The reactor will then be maintained at approximately constant reactivity (and therefore constant temperature) by the inherent nuclear effects designed into the system. A typical average coolant temperature vs time curve for 1-yr of SNAP 10A operation is shown in Figure 18.

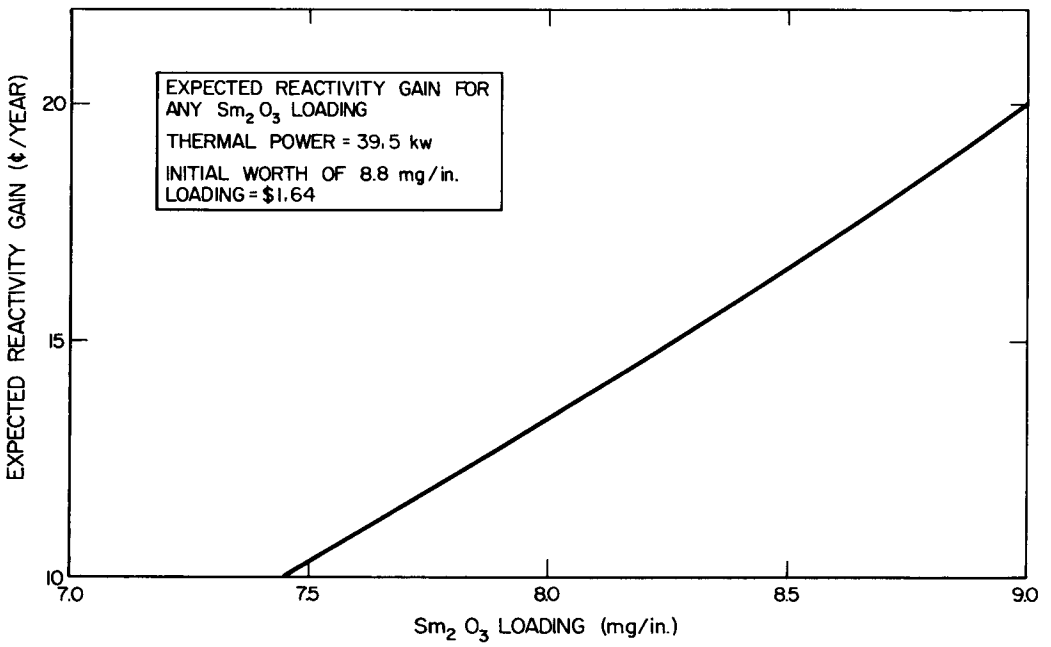

5-26-64 7623-0303

Figure 17. Expected Reactivity Gain for any Sm_2O_3 Prepoison Loading

The temperature drops rapidly during the first month of static operation due to the relatively large reactivity loss accompanying completion of hydrogen redistribution. Over the remainder of the year, however, the positive reactivity effect achieved through burnout of samarium prepoison more than balances long-term reactivity losses and the reactor coolant temperature rises slowly, approaching its initial value.

a. Transient Analyses

The most critical portion of reactor startup occurs when the reactor first becomes supercritical. Since the reactor power level is very low ($\sim 10^{-12}$ watt) when reactivity insertion is initiated, heat generation and temperature feedback effects are negligible during the early stages of reactor startup. When the reactor becomes critical the power level is increasing exponentially. Analyses indicate that several reactivity insertion steps are taken after the effective neutron multiplication (k_{eff}) becomes greater than one and before negative temperature feedback effects such as fuel expansion, spectral effects, etc. cause the power rise to be reversed.

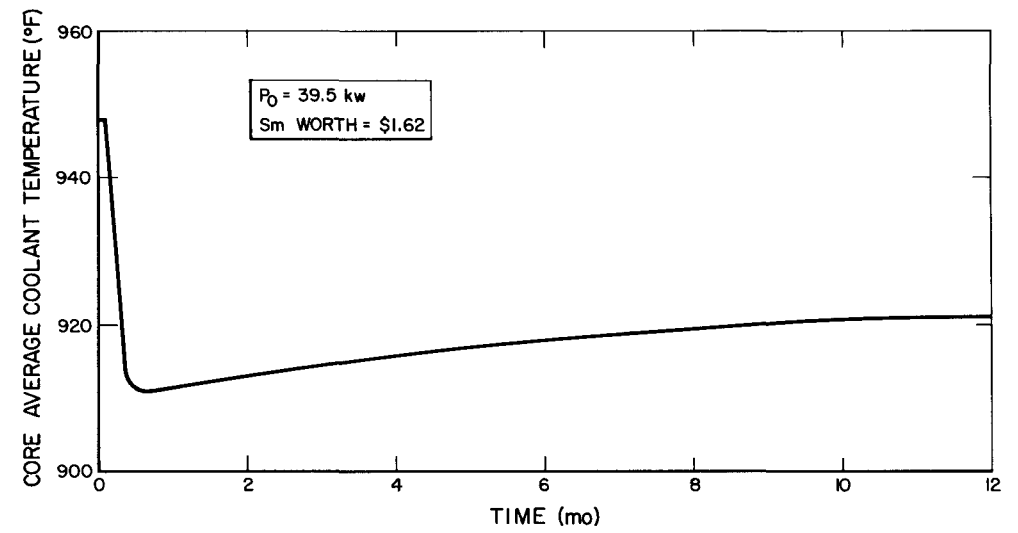

6-12-64 7623-0304

Figure 18. Predicted SNAP 10A Reactor Outlet Temperature Drift vs Time

Analyses of this power transient have been made by both digital and analog techniques.[27] The results computed using these two methods have been in good agreement. The studies indicate that the peak power attained in the transient is controlled primarily by the prompt fuel coefficient. The prompt fuel coefficient employed in the transient analysis study ($\alpha_F \simeq -0.055¢/°F$) was the minimum value which could be inferred from the overall isothermal temperature coefficient measured during the S10FS-1 tests. Use of a minimum prompt fuel coefficient results in a pessimistically large startup transient. The source power level and initial coolant temperature also influence the magnitude of the transient and the rate at which it occurs. The results of the digital analysis are shown in Figure 19.

The ultimate mode of fuel element failure during a startup transient has been determined to be cracking of the ceramic hydrogen barrier at the junction of the cladding tube and the top end cap. The predicted rate of change of NaK coolant outlet temperature above which cracking may occur is 11°F/sec. The expected maximum rate of change of outlet temperature during a normal SNAP 10A startup is between 1.6 and 2.4°F/sec.[28] On this basis, it has been concluded that no element failure should occur during the SNAP 10A startup transient.

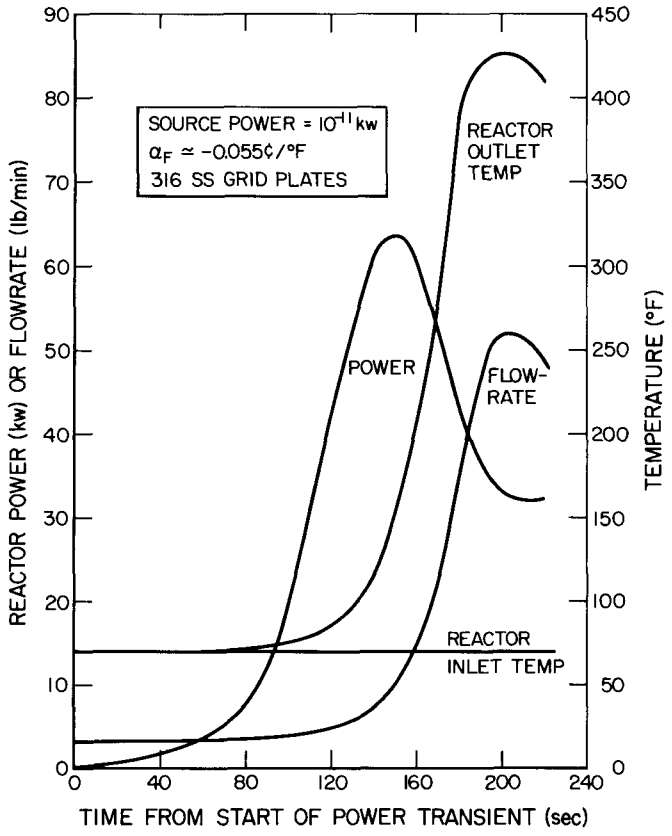

6-12-64 7623-0305

Figure 19. SNAP 10A Initial Startup Transient

b. Effective Delayed Neutron Fraction and Prompt Neutron Lifetime for SNAP 10A

A calculation was made of β_{eff}, the effective delayed neutron fraction, and ℓ, the prompt neutron lifetime. The value of the ratio (β_{eff}/ℓ) determines the dynamic response of the reactor to reactivity insertions. β_{eff} was determined by calculating the change in k_{eff} which occurred when the delayed neutron fraction (energy range 0.017 to 0.90 Mev) was removed from the fission neutron source term in the multigroup calculation. The following equation relates the resulting change in k_{eff} to β_{eff}.

$$\beta_{eff} = (1 - \beta)\frac{\Delta k_{eff}}{k_{eff}} \qquad \ldots(11)$$

where,

β = delayed neutron fraction for U^{235}

Δk_{eff} = difference in calculated multiplication constant between case in which all neutrons are considered and case in which only prompt neutrons are considered.

k_{eff} = multiplication constant considering only prompt neutrons.

For the prompt neutron lifetime calculation, k_{eff} was varied by adding different amounts of an absorber (natural boron) to the calculational model. The relationship between neutron lifetime and changes in neutron absorption is shown in the following equation.

$$\ell = \frac{k_{eff} - k'_{eff}}{\Delta \Sigma a_i V_i k_{eff} k'_{eff}} \qquad \ldots(12)$$

where

k_{eff} = unperturbed multiplication constant

k'_{eff} = perturbed multiplication constant (after boron addition)

$\Delta \Sigma_{a_i}$ = perturbation in absorption cross section due to boron addition

V_i = neutron velocity

The calculated results are compiled in Table 11. The calculations were made with several reflector thicknesses to determine the effect of additional reflector on β_{eff}/ℓ.

The β_{eff}/ℓ ratio for the SCA-4C reactor was measured by noise analysis techniques. The value of β_{eff}/ℓ obtained was 1380 sec^{-1} which is in good agreement with calculated results. This value indicates a prompt neutron lifetime of 5.8 μsec if a value of 0.008 is taken for β_{eff}.[29]

TABLE 11

COMPARISON OF CALCULATED* AND EXPERIMENTAL VALUES OF β_{eff}/ℓ FOR SNAP 10A

β_{eff} Calculation		Prompt Neutron Lifetime Calculation			
K_{eff} vs Reflector Size	β_{eff}	K_{eff} vs Reflector Size	K_{eff} vs Boron Concentration	ℓ (μsec)	β_{eff}/ℓ (sec^{-1})
0.9915	0.00813	0.9946	0.9942	5.40	1506
1.0073	0.008083	1.0103	1.0099	5.68	1424
1.0212	0.00806	1.0243	1.0239	5.88	1372
1.0398	0.00803	1.0428	1.0424	6.13	1310
1.0556	0.00800	1.0586	1.0581	6.62	1208
1.0730	0.00794	1.0760	1.0755	7.31	1087

*AIM-6 Multigroup Calculation
SCA-4C Noise Analysis Measurement of $\beta_{eff}/\ell = 1380\ sec^{-1}$

D. MISCELLANEOUS REACTIVITY EFFECTS

Two general methods may be employed for final adjustment of SNAP 10A reactivity to the required cold, clean excess value. These are: (1) variation of the core composition, particularly the moderator concentration and (2) change of the effective reflector thickness. The hydrogen moderator concentration may be varied by placing one or more "low N_H" elements (i.e., elements with ~95% of nominal element hydrogen concentration), in various locations in the reactor core. SCA-4C experiments have shown that each substitution of a low N_H element for a nominal element reduces reactivity by ~18¢ at the core center and ~6¢ at the core edge. Selective placement of these elements therefore permits relatively fine adjustments in core reactivity.

At one time, consideration was also given to use of beryllium dummy rods for adjustment of core reactivity. These rods were fabricated from beryllium and were identical in outer dimensions with nominal fuel elements. However, SCA-4C critical experiments indicated that replacement of a fuel element with a beryllium dummy rod would reduce reactivity by a minimum of 65¢. Reactivity adjustment using this approach was therefore considered to be too coarse to be of practical interest for the SNAP 10A reactor.

After the reactor has been fully loaded with fuel, and the excess reactivity measured, it may be necessary to adjust the excess reactivity to obtain the desired excess of $3.00. The reactor is designed so that the thickness of the reflector, and therefore system reactivity, may be adjusted by adding or removing beryllium shims. Shims can be added to all control drums and to two of the four reflector surfaces. When the reactor is initially loaded with fuel, it is planned to have one full set of shims attached to all available reflector external surfaces. Up to three full sets of reflector shims may be added, if necessary. However, a full shim set does not have to be added in one step. The criteria for shimming is that the center of gravity of the reactor system should not be disturbed by the structural change. This restriction requires the addition of an equal number of shims to opposite sides of the reflector during each shimming operation.

The worths of these shims, which are essentially 1/8 in. thick slabs of metallic beryllium, were measured on the SCA-4C reactor. The addition of each set provided an average of approximately 42¢ of reactivity. It was estimated

that the shims on the control drums were worth about 8¢ apiece and that smaller shims on two sides of the reflector block were worth about 6¢ each.

The chart in Figure 20 shows the total excess reactivity and the amount of active control (worth of the two fine control drums) which was available as shims were added to the SCA-4C critical assembly. As shims are added on the active control drums, the new reactivity values are read from left to right on the chart, and as shims are added on the passive drums and two sides of the stationary block reflector, the new reactivity values are read from bottom to top. The diagonal of this reactivity worth matrix contains the values for the addition of complete sets of shims.

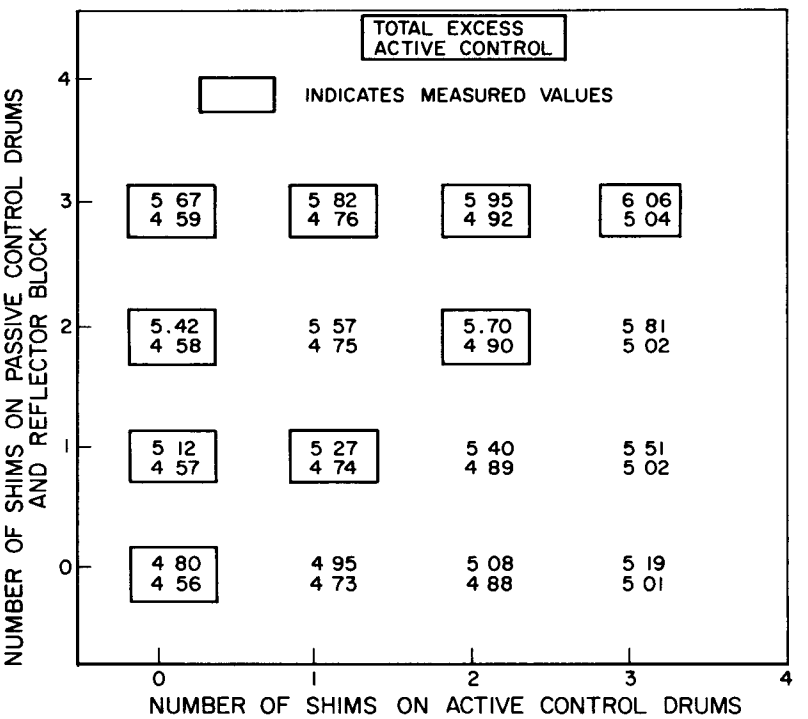

5-26-64 7623-0306

Figure 20. SCA-4C Control Drum Worths and Excess Reactivity

1. Reflector and Control Drum Worths

The SNAP 10A reactor utilizes reduction in neutron leakage as the primary reactor control mechanism during the active-control period. The reactivity worth of the control drums is, therefore, one of the more important parameters measured in SNAP critical assemblies. Calculation and measurement of control drum and reflector worth are discussed on the following page.

Results of an AIM-6 calculation of SNAP 10A reactivity vs cylindericized reflector thickness are shown in Figure 21. The figure may be used to predict the approximate change in reactivity when reflector shims are added. In order to estimate shim worth it is necessary to calculate an "effective" shim thickness which accounts for the fact that shims are not added in an idealized geometrical manner. It was determined that a full set of six 1/8-in. thick shims added to all shimmable surfaces was approximately equal to 0.07 in. (~0.18 cm) of idealized thickness. When this dimension is added to the idealized SNAP 10A reflector thickness of ~5.5 cm, the figure indicates that the reactivity worth (of one set of shims) is 47.5¢. A one-shim set worth of 47¢ was measured in the SCA-4C reactor. The worth of three complete sets of shims is calculated as $1.30, compared to $1.26 as measured in the SCA-4C critical assembly.

A typical experimentally determined SNAP 10A control drum calibration curve, (i. e., a plot of drum worth vs drum rotation), is shown in Figure 22. In general, it has been found that drum worth does not change significantly when the reactor core flux shape is changed. Drums were calibrated in the SCA-4C assembly with various core loadings, some of which lowered reactivity by as much as $3.00 from the base case, and involved substantial flux perturbations. Measured changes in drum worth were less than ±3%, well within the limits of experimental error. Control drum calibration curves based on critical experiments were used exclusively in SNAP 10A analyses, since reliable analytical methods for estimation of drum worth are not currently available.

2. Gridplate and Other Material Worths

The relative reactivity worths of various proposed gridplate materials have been measured in the SCA-4C critical assembly and calculated using the AIM-6 code. The materials investigated were Hastelloy-C, Carpenter low expansion alloy 42 (similar to Invar), and 316 SS. The standard reference gridplate for the SCA-4C critical assembly is fabricated from 316 SS and contains penetrations only for fuel rod indexing pins. The flight design LE 42 and Hastelloy-C gridplates contain holes for coolant flow as well as pin indexing penetrations. The amount of material present in the flight design plates is therefore about 20% lower than in the SCA-4C plates. Critical assembly measurements showed the LE 42 and Hastelloy-C upper gridplates to be worth ~3¢ more than the SCA-4C stainless steel upper gridplate. An AIM-6 calculation of relative gridplate worths indicated that the 316 SS plate would be ~0.4¢

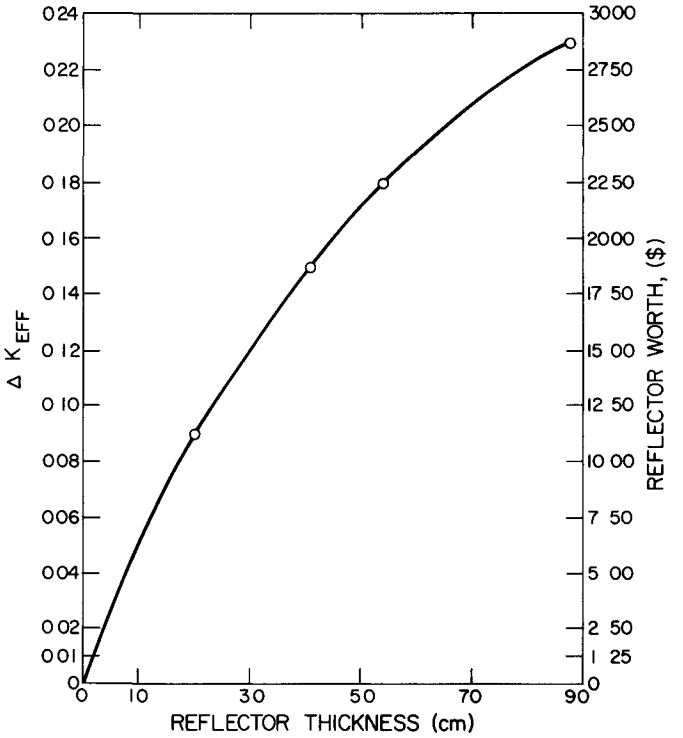

5-26-64 7623-0307

Figure 21. Change in Reactivity Due to Varying SNAP 10A Reflector Thickness

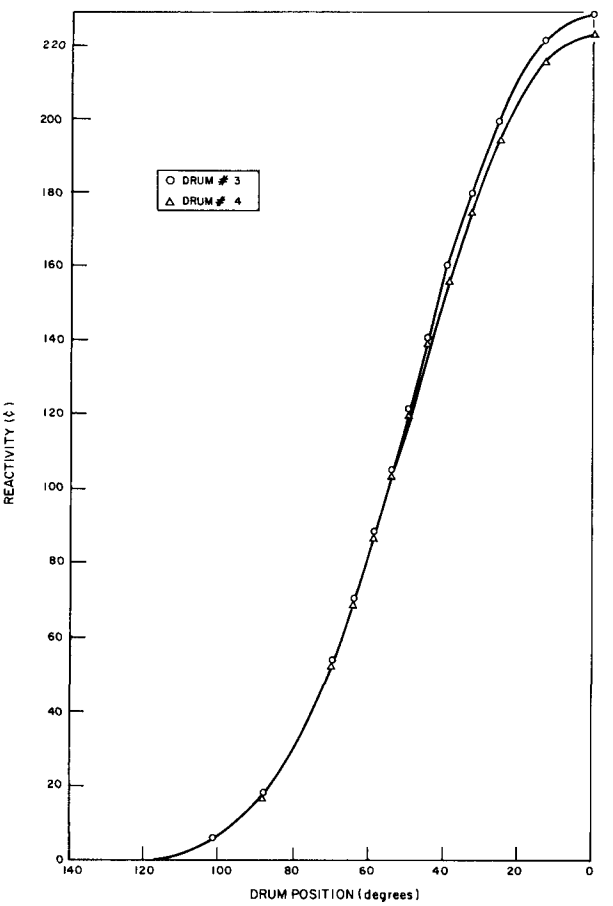

5-1-64 7623-0281

Figure 22. SNAP 10A Reactor Control Drum Worth vs Control Drum Position

more reactive than the LE 42 plate. Within the limits of experimental and calculational error, it can be concluded that the difference in worth of various proposed gridplate materials is negligible.

A series of nuclear tests designed to measure the worth of hydrogen has been completed using SNAP 10A fuel elements in the SCA-4A critical assembly. The difference in reactivity which resulted when fuel elements with slightly different values of N_H were substituted for elements of known hydrogen content was measured in various core positions. These measurements indicated that the average worth of hydrogen in the reactor was \$1.00/0.1 N_H unit. The best analytical prediction of hydrogen worth, made using AIM-6, is \$0.95/0.1 N_H unit. The core center element hydrogen is calculated to be worth 5.2¢/0.1 N_H unit.

The worth of samarium has been calculated and measured experimentally as described in the previous sections. The worth of the remaining major fuel constituents has been calculated using the DTK and AIM-6 codes. The incremental worths of zirconium, U^{235}, Hastelloy-N cladding, and carbon and boron fuel impurities have been calculated. Results are summarized in Table 12.

TABLE 12

INCREMENTAL NUCLEAR WORTHS OF VARIOUS MATERIALS IN THE SNAP 10A CORE

Material	Incremental Worth
Zirconium	+19¢ per 1% Δw/w change
U^{235}	+9.1¢ per 1% Δw/w change
Hastelloy-N	-1.2¢ per 1% Δw/w change
Carbon	~+0.8¢ per 100 ppm change
Natural boron	~-3¢ per 1 ppm change

It should be noted that the incremental worths quoted are valid only at or near the nominal reactor composition. Several of the nuclear worth estimates presented in Table 12 have not been verified experimentally. However, the

fact that the calculated worths of hydrogen and samarium are in good agreement with experiments indicates that calculated worths of other core constituents are reasonably reliable.

3. Environmental Differences Between Testing Facility Buildings

Individual fuel elements and complete core loadings for SNAP 10A reactors have been calibrated in the SCA-4 critical assembly in Building 373, Santa Susana. Present plans call for both flight reactors (SNAP 10FS-4 and FS-5) to be loaded with fuel and tested at low power in Building 019, Santa Susana. Startup and full power operation tests will also be carried out on SNAP 10FS-3 in Building 024, Santa Susana. The three buildings present different environments due to differences in the size of the vaults, presence or absence of vacuum chambers, surrounding equipment, etc. Because of the environmental differences, the reactivity measured for a given system will vary slightly from facility to facility. These measured reactivities will in turn differ from those observed in flight. Facility differences and their effect on reactivity are discussed below.

The SCA-4C and SCA-4A reactors were located in a corner of the vault in Building 373. The two walls closest to the reactor are 40 and 48 in., respectively, from the center axis of the reactor. In Building 019, the center axis of the reactor is about 72 in. from the vault walls and the reactor is enclosed in a large, cooled vacuum chamber fabricated of carbon steel. The vault in Building 024 is approximately 15 feet square; the prototype flight system is sealed within a cooled vacuum chamber fabricated from aluminum alloy and located at the center of the vault.

Two different approaches were taken in attempts to estimate the reactivity effects of these vaults. The first approach was a theoretical one using the SNG transport theory code. Vault worths calculated using this approach were known to be overestimates because the models used to represent the vaults were chosen with radii equal to the minimum distance from the reactor center to a vault wall.

The second approach was to combine experimental results from SCA-4C experiments with geometrical scaling factors. These scaling factors were used to extrapolate experimental worth measurements to the reactor-vault configurations being studied. This approach used results of experiments in which the

SCA-4C reactor was surrounded in turn by lucite, concrete, iron and aluminum blocks. The worth of each of these materials was determined at one or more distances from the reactor surface. The rings of material varied in thickness, but were all about 18-in. high.

The experimental results were plotted in terms of ring radius vs reactivity worth. The curves were extrapolated assuming reactivity to be functions of $1/R^2$ and $1/R^3$, where R is vault radius. A scaling factor was used to take into account the noncylindrical geometry of the vault. The factor was derived by considering (a) the ratio (β) of neutrons which leave the vault wall to those that strike it, and (b) the fraction of neutrons which strike the reactor upon returning from the vault wall.

Reactivity effects were estimated using the equation,

$$\Delta\rho = \frac{\beta\left(1 - \sqrt{1 - \frac{r^2}{R^2}}\right)}{1 - \beta\sqrt{1 - \frac{r^2}{R^2}}} \qquad \ldots(13)$$

where

$\Delta\rho$ = change in reactivity

r = reactor radius

R = vault radius

Vault worths estimated using the two approaches are compared in Table 13. As noted earlier, the SNG calculations represent upper limits for vault worth. The extrapolated experimental values are believed to be much more realistic. However, uncertainties also exist in these values due to the fact that each ring measured was only 18-in. high while, in reality, the vault materials completely surround the reactor. Also, the concrete used in the experiment was different in composition from that used for construction of the vault. Exact differences in concrete composition are not known, but there are indications that there is more water (neutron scatterer) in the vault concrete than in the experimental blocks.

TABLE 13

CALCULATED VAULT WORTHS FROM THE SNG CALCULATION AND SCA-4C EXTRAPOLATION METHOD (30)

Facility	SNG Calculations (¢)	SCA-4C Extrapolation Method (¢)	
		Total Vault*	Vacuum Chamber Only
Building 373	+55	+2.5	-
Building 019	+25	+5.1	+1.8
Building 024	+21	+3.3	+1.2

*Includes vacuum chamber

In addition to vault worth differences, other environmental differences exist and include size differences between ground and flight system reflectors, NaK in core and plenums, a NaK pump and top head, and the fact that the critical assembly utilizes a supporting table and reflector drive machinery and is operated dry while the reactor tests employ a neutron shield.

The total worth of the NaK in the core and plenum chambers was originally calculated to be -$0.09 ± $0.10. The calculation was made using the DTK transport theory code. NaK worth is difficult to calculate reliably due to uncertainties in methods for treatment of transverse neutron leakage from the plenum regions. Recent calculations made using the DDK two-dimensional transport theory code, which more accurately accounts for changes in axial neutron streaming, predicts SNAP 10A NaK worth to be +17¢ ± 8¢.

NaK worth in S2DR was determined experimentally to be +3 ± 10¢. There was actually about a 16¢ increase in reactivity when NaK was first added to the dry system. However, most of this change was due to filling of the NaK return pipe adjacent to the vessel. An aluminum bar in the same location produced about a +13¢ change in reactivity. NaK worth in the core and plenum regions was therefore estimated to be +3¢, with a ±10¢ uncertainty band due to experimental error. Since the S2DR employed BeO axial reflectors while SNAP 10A does not, NaK plenum worths would be expected to differ for the two reactors.

The worth of NaK was also measured in the course of low-power S10FS-1 ground tests. Total worth of NaK in core and plenums was estimated to be +26¢ ± 0.5¢.

The total worth of the lithium hydride neutron shield was estimated, using SCA-4C measurements of LiH worth at various positions, to be +$0.35. NaK pump worth was similarly extrapolated as +$0.10. The worth of aluminum support structure for the SCA-4C reflector and drums was also scaled from the metal ring worth experiments; base plate and surrounding machinery worth was determined in the same manner. Estimated values are $0.46 and $0.25, respectively. A summary of various component and material worths is presented in Table 14.

TABLE 14

ESTIMATED AND MEASURED ENVIRONMENTAL EFFECTS FOR VARIOUS SNAP 10A REACTOR CONFIGURATIONS

Environmental Effect	Nuclear Worth (¢)	Method Estimating Worth
1. NaK in core and plenum (flight) systems - Building 019 and 024)	-9 ± 10 +3 ± 10 +17 ± 8 +26 ± 0.5	DTK calculation S2DR measurement DDK calculation S10FS-1 measurement
2. LiH shield (flight systems - Buildings 019 and 024)	+35 ± 10	Extrapolation from SCA-4 measurements
3. Top head (flight systems - Buildings 019 and 024)	+ ~ 10	Extrapolation from SCA-4 measurements
4. Aluminum support for reflector and drums (SCA-4C - Building 373)	+46 ± 20	Extrapolation from SCA-4 measurements
5. Steel base plate and machinery (SCA-4A and SCA-4C - Building 373)	+25 ± 10	Extrapolation from SCA-4 measurements

The SCA-4C critical assembly and S10FS-1 ground prototype reflectors were essentially identical in all dimensions. However, the S10FS-3, -4, and -5 reactors employ a reactor vessel-reflector gap 10 mil larger than the gaps of the other two reactors and reflector worth is slightly reduced. The nuclear worth of beryllium removal from the inner surface of the reflector has been calculated using the AIM-6 code and has also been measured in the SCA-4A critical assembly. The measured worth was 2 ± 0.5¢/mil of beryllium, while the calculated value was 2.5¢/mil of beryllium. On the basis of the SCA-4C experimental data, worth of the S10FS-3, -4, and -5 reflectors is estimated to be 20 ± 5¢ lower than S10FS-1 and SCA-4C reflector worths.

E. SAFETY DEFICES AND EXPERIMENTS

In addition to analysis of the static and kinetic characteristics of the SNAP 10A reactor, analyses of hazards during handling operations have been completed.

A discussion of the handling operations and hazards involved in transporting the reactor to the launch site may be found in Reference 31. The following sections provide a description of the shipping sleeve, which replaces the reflector during shipment, and the void filler blocks, which prevent accidental control drum insertion while the reflector is attached to the reactor during various ground handling operations. The experiments performed to demonstrate the effectiveness of these devices, and to determine the nuclear hazards associated with men working on or in the vicinity of the reactor, are also discussed.

1. Shipping Sleeves and Void Filler Blocks

A bare SNAP 10A reactor is supercritical when submerged in water. During interfacility reactor shipment, it is conceivable that the reactor could be dropped on a hard surface and/or be submerged in water. It is also possible that the body of a man working on or around the reactor could act as a reflector and cause a nuclear accident. To ensure against these circumstances, two safety devices have been designed and tested: (a) the shipping sleeve which is used when the reactor is being transported between facilities, and (b) the void filler blocks which are employed whenever the reflector is attached to the reactor during various ground tests.

The shipping sleeve is an annular stainless steel device containing void and poison regions. The sleeve surrounds the radial surface of the reactor, replacing the beryllium reflector (see Figure 23). The inner radial portion of the sleeve is essentially a void about 3-3/4 in. thick. Outside the void region is a peripheral section about 1-in. thick and containing boron powder.

In selecting a shipping sleeve configuration capable of providing maximum negative reactivity when immersed in water, both the neutron reflection and neutron absorption properties of the materials comprising the sleeve must be considered. The positive reactivity effect of water surrounding the reactor is due primarily to neutron thermalization and subsequent reflection of thermal neutrons back into the core. Thermal neutron absorbers such as boron, placed directly outside the core, will absorb most of the reflected neutrons. However, many materials, including boron, are more effective than water as reflectors of epithermal neutrons. Thus, use of a neutron absorber in the sleeve will result in both increased reflection of higher energy neutrons and decreased return of thermal neutrons to the reactor core. For each particular void width

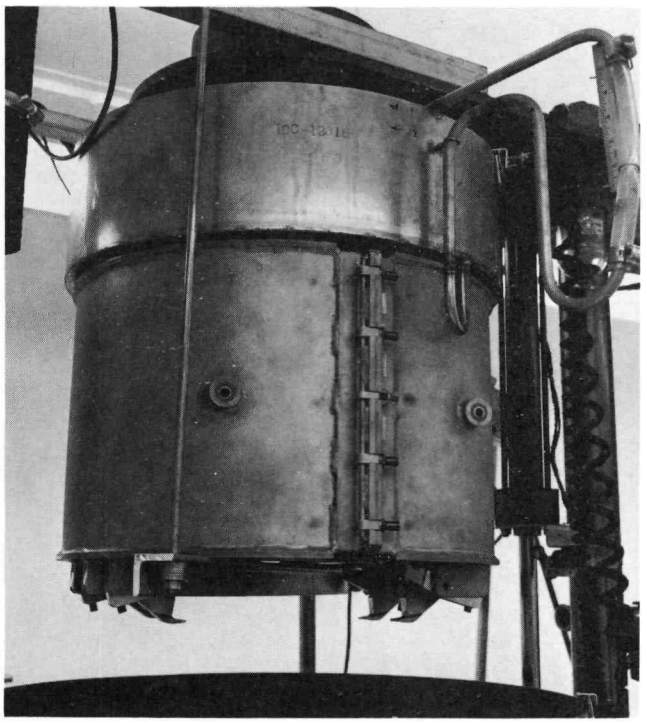

8-1-63 7611-4602

Figure 23. SNAP 10A Reactor With Shipping Sleeve Attached

there is an associated optimum thickness of absorber which provides a shipping sleeve of maximum negative reactivity. When absorber thickness is decreased below the optimum, an increased number of thermal neutrons return to the core. With more than optimum absorber thickness, more epithermal and fast neutrons are reflected to the core.

The reactivity of the reactor and shipping sleeve submerged in water was calculated with the AIM-6 diffusion code assuming several thicknesses of various neutron absorbing materials. Boron was selected as the most promising neutron absorber because of its relatively high thermal and epithermal neutron absorption cross sections.

Effectiveness of a shipping sleeve of optimum design was determined experimentally in the SCA-4B critical assembly. Several experiments were performed. In the first, the shipping sleeve was attached to the reactor vessel, the core was loaded with 31 SNAP 10A FS-1 fuel elements and 6 lucite dummy elements, and the core was filled with water. The reactor and sleeve were then totally immersed in water and the reactivity was measured. This procedure was repeated with three of the lucite rods replaced by three fuel elements,

and then repeated again with 37 fuel elements and no lucite rods. Inverse multiplication was plotted against number of fuel elements loaded; the curve was then extrapolated to determine the approximate critical loading. It was estimated that, with a loading of 41.8 ± 1.0 fuel elements, the reactor would achieve criticality. Since the average worth of peripheral fuel element relative to lucite had been measured (in the SCA-4C critical assembly) as $0.55, subcriticality of the reactor-sleeve configuration was estimated to be -$2.64 ± 0.55. Pulsed neutron experiments on the same assembly indicated the reactor to be $3.00 ± 0.50 subcritical.

The shipping sleeve was designed to maintain the flooded and immersed reactor subcritical following an interfacility shipping accident. Drop tests establishing the durability of the device have been conducted. Since it is possible that a shipping accident might also initiate a high temperature NaK fire, the stainless steel sleeve has also been designed to withstand external temperatures up to 2000°F.

The void filler blocks are employed to ensure that the reactor will remain subcritical during all conceivable handling accidents which might occur while the reflector is attached to the reactor. Basically the void filler blocks are void-poison devices which fit into the control drum voids and surround the external reflector surface. An inner boron region about 1/2-in. thick is adjacent to the beryllium. The remainder of the block consists essentially of a void region encased in stainless steel (see Figure 24).

The void filler blocks are designed primarily to avoid accidental criticality due to human reflection during ground testing of the reflected reactor. The blocks are also designed to ensure subcriticality of a water-surrounded, beryllium-reflected, NaK-filled reactor. The filler blocks are not designed to keep the reflector reactor subcritical with water both inside the core and outside the reflector.

Tests have been conducted in the SCA-4B facility to determine the reactivity of the SNAP 10A FS-1 fuel loading in a water-immersed beryllium reflected configuration, with void filler blocks in place. The reactor was found to be $1.32 ± 0.22 subcritical using the extrapolation to criticality methods described in the previous section. Pulsed neutron experiments indicated the

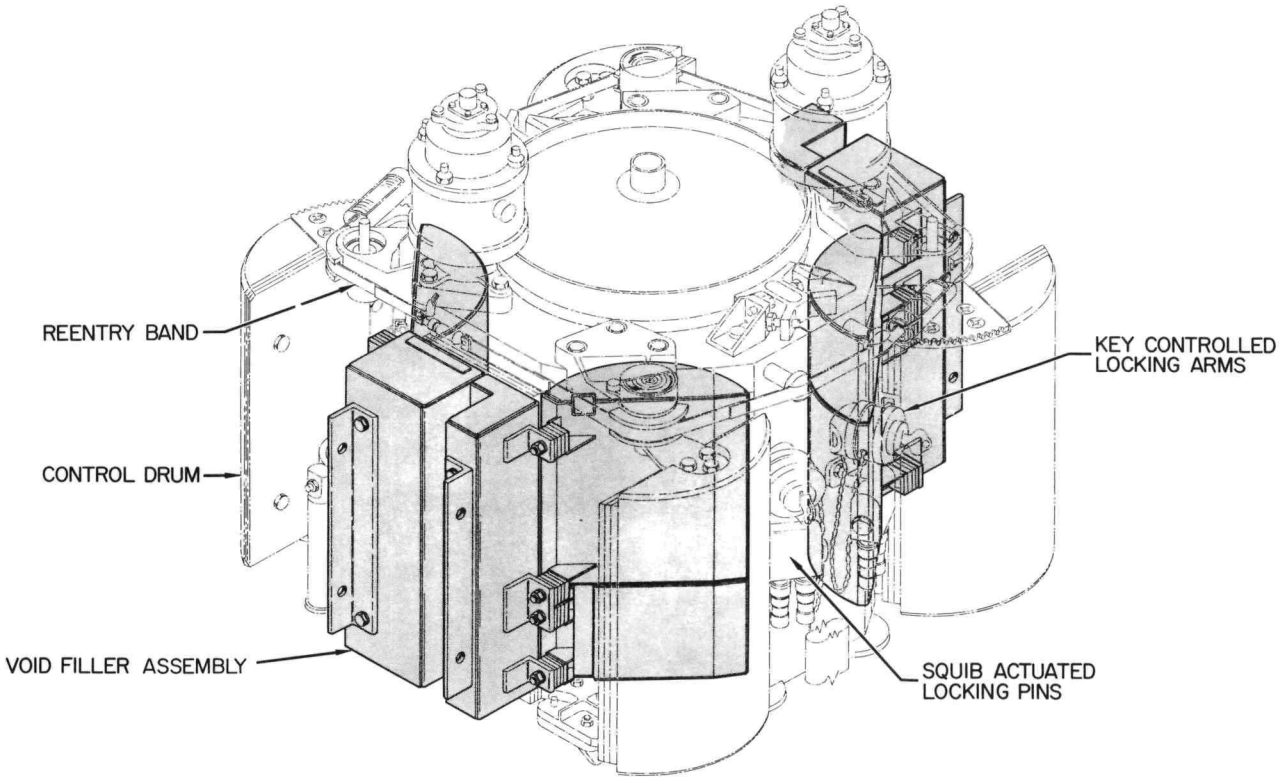

10-21-63 7561-0513C

Figure 24. SNAP 10A Reactor With Void Filler Blocks Attached

reactor to be \$1.49 ± \$0.25 subcritical under the same conditions. A pulsed neutron run was also made without water reflection, but with the beryllium reflector and filler blocks in place. The shutdown margin was estimated to be \$6.00 ± \$1.00 under these conditions.

2. Human Worth Experiments

Due to the small size, relatively low shutdown margin, and high neutron leakage associated with the SNAP 10A reactor, persons working on or near the reactor could conceivably be capable of reflecting sufficient neutrons to produce a critical system. Appropriately, this condition is known as the "fat man" accident. A number of experiments were conducted in the SCA-4C critical assembly in order to establish the approximate nuclear worth of the body of a human being leaning against or standing adjacent to the reactor (Reference 21). Hydrocarbons and plastics, which are good nuclear mockups of the human body, were used in the experiments.

In the first approach, ~80 lb of paraffin was stacked beside or on top of the reflected reactor. The paraffin occupied about 1/8 of the reflector perimeter to full core height, and was about 5 in. in thickness. This arrangement increased reactivity only about 14¢. Paraffin stacked directly on top of the upper gridplate was found to be worth about 90¢.

A second experiment for estimation of maximum human worth consisted of the attachment of lucite shims to all possible reflector surfaces. Measurements indicated lucite shim worth to be about $2.00/in. of added thickness for the configuration studied. Experimental results are not completely applicable to human worth estimates because the human body cannot generally be distributed in the same manner as the shims.

The best approximation to a realistic human mockup consisted of the placement of 200 lb of lucite pellets and paraffin blocks inside a pair of workman's coveralls. This "fat man" was then situated in various positions around and over the SCA-4C core and the reactivity was measured. The most reactive position was found to be one in which the "fat man" was draped over the top of the core with arms wrapped around the reflector. In this position, the human mockup was estimated to be worth about 84¢.

Two pairs of rubber gloves were filled with lucite pellets (~444 gm of lucite in each glove) and were tightly packed into the open drum voids. Their combined worth was determined to be about $1.11. On the basis of these experiments, it was estimated that a human being draped over the top of the reactor with hands in open drum voids could cause a maximum increase in reactivity of $1.95. Results of SCA-4C human mockup experiments are summarized in Table 15.

TABLE 15

SUMMARY OF SCA-4C HUMAN MOCK-UP EXPERIMENTS

Configuration	Worth ($)
80 lb stack of paraffin - beside reflector	+0.14
- above top gridplate	+0.90
1/8 in. thick lucite shims on all shimmable reflector surfaces	+0.25
1/4 in. thick lucite shims on all shimmable reflector surfaces	+0.53
3/8 in. thick lucite shims on all shimmable reflector surfaces	+0.74
200 lb lucite and paraffin "fat man" draped over and around reflected reactor	+0.84
2 lucite "hands" in open drum voids	+1.11

IV. SNAP 10A REACTOR GROUND TEST RESULTS

A. RESULTS OF SNAP 10A FS-1 REACTOR GROUND TEST

The SNAP 10A FS-1 ground test reactor was the first completely integrated SNAP 10A system to commence acceptance testing. Acceptance testing is divided into two phases: structural tests and low power physics tests. The purpose of the tests is to demonstrate the ability of system components to meet the requirements of preflight and orbital environments.

Results of the low power physics tests completed with the S10FS-1 reactor are shown in Table 16. Predicted reactivity values are shown for comparison. The predictions were largely based on SCA-4A critical assembly measurements.

The hot, wet critical test was performed by heating the NaK coolant with "strap-on" electrical heaters. The reactor was manually maintained at critical during the temperature rise and the reactivity defect was determined by recording changes in control drum position with temperature.

The S10FS-1 reactor ground test was terminated shortly before its scheduled completion due to rupture of one NaK expansion compensator. Analysis of the S10 FS-1 nuclear test results is still in progress.

B. SNAP 10A FS-3 REACTOR GROUND TEST

Shortly after termination of the SNAP 10A FS-1 test, the S10 FS-3 reactor system was delivered for acceptance testing. Results of the S10 FS-1 and S10 FSM-1 tests were used as a basis for minor revision of the S10 FS-3 fuel loading, shimming configuration, and samarium prepoison loading. Analysis of the changed fuel loading was completed using methods described in this report, and reactivity predictions were made for S10 FS-3.

The dry critical test has been completed and the results are shown in Table 17.

TABLE 16

LOW POWER PHYSICS TEST COMPLETED WITH SNAP 10 FS-1 REACTOR

	Measurement	Measured Value	Predicted Value
Dry Critical Test	Minimum supercritical fuel loading	32 elements	32 elements
	ρ ex minimum supercritical loading ($)	0.32	0.16
	Cold, dry, zero power ρ ex with 37 element fuel loading ($)	3.53	3.59
	Control drum worth with 1 shim ($)	2.26	2.30
	Worth of change in environment from Building 373 to Building 019 vault ($)	-0.28	-0.25
Wet Critical Test	Worth of NaK coolant in core and plenums ($)	+0.26	-0.09
	ρ ex, cold, wet, 1 shim ($)	3.76	3.50
	Control drum worth with 1 shim ($)	2.23	no estimate
	Control drum worth with no shims ($)	2.15	no estimate
	ρ ex, cold, wet, no shims ($)	3.19	3.03
Hot, Wet, Critical Test	Overall isothermal temperature defect ($)	-2.04	-2.56
	Overall isothermal temperature coefficient		
	70-937 (°F) – (¢/°F)	-0.245	-0.29
	850-950 (°F) – (¢/°F)	-0.29	-0.32

TABLE 17

SNAP 10A FS-3 REACTOR DRY CRITICAL TEST

Measurement	Measured Value	Predicted Value
Minimum critical fuel loading	33 elements	33 elements
ρ ex with 33 elements	$0.16	$0.18
ρ ex with 37 elements	$2.67	$2.70
Average worth of control drums	$2.20	$2.18

REFERENCES

1. A. R. Dayes, NAA-SR-MEMO-9248, "SNAP 10A/2 Nuclear Calculations Model" (November 22, 1963) (SRD)

2. H. P. Flatt and D. C. Baller, NAA Program Description, "The AIM-6 Code" (January 1961) (Internal Document)

3. D. C. Baller, NAA-SR-7137, "The FAIM Code – A Multigroup, One-Dimensional Diffusion Equation Code" (April 15, 1962)

4. D. Vargofcek, NAA-SR-7146, "The ULCER Code – A Multigroup, One-Dimensional Diffusion Equation Code With Upscatter" (1962)

5. B. G. Carlson, T-1-159, "The SN Method and the SNG and SNK Codes" (January 26, 1958)

6. Personal Communication, B. C. Colston, Atomics International with J. Worlton, Los Alamos

7. R. A. Blaine, V. E. Anderson, and B. F. Mashowitz, AMTD-167, "BAM, A Code to Compute Thermal Group Constants" (August 1962) (Internal Document)

8. H. P. Flatt and D. P. Satkus, NAA Program Description, "SIZZLE" (Feburary 1961) (Internal Document)

9. W. A. Rhoades, NAA-SR-MEMO-7515, "The QUICKIE Code – A Multigroup Reactivity Calculation for One-Region Systems" (June 22, 1962)

10. R. W. Winson, NAA-SR-7322, "HYTRAN – A Hydrogen Diffusion Code" (April 16, 1962)

11. The HYLO Code, Personal Communication with K. R. Birney and D. J. McGoff, Atomics International

12. J. D. Watrous, and M. E. Nathan, NAA-SR-MEMO-8520, "Fuel Element Parametric Study Advance SNAP 2 Reactor" (July 10, 1963)

13. NAA-SR-MEMO-8520, Ibid, Addendum 1

14. NAA-SR-8295, "Final Report S2DR Test Program" (to be issued)

15. J. P. Beall, and M. W. Hulin (Editors), NAA-SR-7088, "The Final Report on the SNAP 2 Experimental Reactor (SER) Operation and Test Program" (April 30, 1962)

16. R. Brehm, NAA-SR-MEMO-7011, "Summary Hazards Report and Operations Manual for SNAP Critical Assemblies 4-A and 4-C" (January 22, 1962)

17. L. I. Moss, NAA-SR-MEMO-8490, "Experiments with Water-Reflected Undermoderated, Zirconium Hydride Critical Assemblies" (to be published)

REFERENCES

18. D. F. Paddleford and R. W. Winson, NAA-SR-MEMO-8325, S10FS-1 Accident Analysis" (March 19, 1963)

19. R. Hart, NAA-SR-MEMO-7582, "Factory to Flight Nuclear Safety in SNAP 10A/2 Program (to be issued)

20. J. Miller, W. J. Roberts, and R. L. Brehm, NAA-SR-7140, "Temperature Coefficient Analysis for SNAP Reactors" (December 30, 1962)

21. D. W. Clifford, NAA-SR-8613, "Final Report on the SNAP 10A Prototype Critical Assembly Studies" (April 30, 1964)(Confidential)

22. D. F. Paddleford, NAA-SR-MEMO-8822, "SNAP 10A-FR Reflector Coefficient of Reactivity" (July 24, 1963) (Confidential)

23. R. N. Stuart et al., UCRL-5293, "ZOOM – A One-Dimensional Multigroup Neutron Diffusion Theory Reactor Code for the IBM-704" (November 19, 1958)

24. F. Clark et al., NAA-SR-5890, "Analysis of S2DR Design" (June 1, 1961)

25. H. Baucom, NAA-SR-MEMO-6725, "SNAP 10A Prepoisoning" (September 6, 1961) (SRD)

26. J. Blomeke and M. Todd, ORNL-2127, "Uranium-235 Fission Product Production as a Function of Thermal Neutron Flux, Irradiation Time, and Decay Time. Part 1, Atomic Concentrations and Gross Totals"

27. P. M. Magee, NAA-SR-MEMO-9589, "TRANCORE - 10A" (March 5, 1964)

28. P. M. Magee, NAA-SR-MEMO-9195, "Expected Performance of SNAP 10A-FS-1 During First Preliminary Startup Test Including the Effect of Source Level Variations" (November 14, 1963)

29. R. H. Norman, NAA-SR-TDR-8002, "Calculation of β_{eff} and ℓ for SNAP 2/10A" (December 6, 1962)

30. C. Steichen, NAA-SR-7635, "Estimates of the Reactivity Contributions of Vaults Housing the SCA-4C and SNAP 10A Flight System Reactors" (August 13, 1962)

31. R. Hart, NAA-SR-7774, "SNAP 10A Flight Test Final Safeguards Report" (April 1, 1963)

32. E. Faelton and L. Swenson, NAA-SR-TDR to be issued

33. H. E. Johnson, NAA-SR-9295, Hydrogen Dissociation Pressures of Modified SNAP Fuels (March 15, 1964)(Confidential)

34. W. A. Flynn, R. J. Thomson, NAA-SR-9647, "SNAP Radiation Shield Analysis, October 15, 1964.